

# Small-angle scattering behavior of thread-like and film-like systems

Salvino Ciccariello<sup>a</sup>, Pietro Riello<sup>b</sup> and Alvisè Benedetti<sup>b</sup>

<sup>a</sup>Università di Padova, Dipartimento di Fisica G. Galilei, Via Marzolo 8, I-35131 Padova, Italy, and <sup>b</sup>Università Cà Foscari Venezia, Department of Molecular Sciences and Nanosystems, Via Torino 155/B, I-30172 Venezia, Italy. salvino.ciccariello@unipd.it

November 26, 2015

## Abstract

Film-like and thread-like systems are respectively defined by the property that one of the constituting homogenous phases has a constant thickness ( $\delta$ ) or a constant normal section (of largest chord  $\delta$ ). The stick probability function of this phase, in the limit  $\delta \rightarrow 0$ , naturally leads to the definition of the correlation function (CF) of a surface or of a curve. This CF fairly approximates the generating stick probability function in the range of distances larger than  $\delta$ . The surface and the curve CFs respectively behave as  $1/r$  and as  $1/r^2$  as  $r$  approaches to zero. This result implies that the relevant small-angle scattering intensities behave as  $\mathcal{P}_S/q^2$  or as  $\mathcal{P}_C/q$  in an intermediate range of the scattering vector ( $q$ ) and as  $\mathcal{P}/q^4$  in the outermost  $q$ -range. Similarly to  $\mathcal{P}$ , pre-factors  $\mathcal{P}_S$  and  $\mathcal{P}_C$  simply depend on some structural parameters. Depending on the scale resolution it may happen that a given sample looks thread-like at large scale, film-like at small scale and particulate at a finer one. An explicit example is reported. To practically illustrate the above results, the surface and the curve CFs of some simple geometrical shapes have been explicitly evaluated. In particular, the CF of the right circular cylinder is explicitly evaluated. Its limits, as the height or the diameter the cylinder approaches zero, are shown to coincide with the CFs of a circle and of a linear segment, respectively.

*Synopsis: The scattering intensities of thread-like and film-like systems respectively behave as  $\mathcal{P}_C/q$  and  $\mathcal{P}_S/q^2$  in an intermediate range of the scattering vector  $q$ . The  $\mathcal{P}_C$  and  $\mathcal{P}_S$  expressions are reported.*

Keywords: film-like systems, thread-like systems, surface correlation function, curve correlation functions, scale resolution, small-angle scattering intensity behavior

# 1 Introduction

Materials characterized by one film-like or by one thread-like phase are since long known. Examples of the first kind are vesicles in solutions or oil-water-surfactant systems. Examples of the second kind are polymers or amyloid proto-filaments (Avdeev *et al.*, 2013) in solution. Small-angle scattering (SAS) is one the most suitable tools to characterize these materials when the film thickness or the thread diameter is of the nanometer order. In fact, based on the knowledge that the SAS intensity  $[I(q)]$  of a circular cylinder decreases, at intermediate scattering vector ( $q$ ) values, as  $1/q^2$  or as  $1/q$  depending on whether the cylinder's radius is much larger or much smaller than its height (Porod, 1982; Kirste & Oberthür, 1982), one looks for the existence of a plateau in the plot of  $q^2 I(q)$  or of  $q I(q)$  versus  $q$  to conclude that the sample respectively contains (*plane*) flat particles or (*straight*) rod-like ones. Actually this conclusion has a more general validity since it also applies to the cases of *curved* film-like and thread-like phases. To the authors' knowledge, a first attempt to get this more general result, starting from the basic equations of SAS theory (Guinier & Fournet, 1955; Kostorz, 1979; Feigin & Svergun, 1987), was done by Teubner (1990) in the film-like case.

To make this derivation more detailed as well as to extend it to the thread-like case is the aim of this paper according to the following plan. Section 2 reports the basic definitions and results of SAS theory for three phase samples. Section 3 considers the case where one of the constituting phases is a film of thickness  $\delta$ . One shows how the limit  $\delta \rightarrow 0$  of the stick probability function (SPF) of the film-like phase leads to the definition of a *surface correlation function*  $[\gamma_S(r)]$ . This  $\gamma_S(r)$  function fairly approximates the generating SPF in the range  $r > \delta$  and it behaves as  $1/r$  at small distances. Furthermore, the surface CF is explicitly evaluated in the case of a sphere (§ 3.4.1), a circle (§ 3.4.2), a rectangle (§ 3.4.3) and a cubic surface (appendix B). The circle is the limit of a right circular cylinder as the cylinder's height goes to zero. Hence, the corresponding limit of the cylinder CF must coincide with that of the circle. To verify this point one needs to know the explicit expression of the cylinder CF while the only chord-length distribution is presently known (Gille, 2014). This CF calculation is performed in closed form in terms of two elliptic integral functions (see appendix A). Section 4 analyzes the case of a thread-like phase. In the limit of vanishing thread diameter, the corresponding limit of the relevant SPF leads to the definition of the *curve correlation function*  $[\gamma_C(r)]$  that behaves as  $1/r^2$  as  $r \rightarrow 0$  and fairly approximates the considered SPF if  $r > \delta$ . The curve CFs of a linear segment and a circle are explicitly worked out in § 4.1.1 and § 4.1.2. In § 4.1.1 one also shows that the linear segment CF coincides with the limit of the cylinder CF as the cylin-

der's radius goes to zero. The behaviors of the scattering intensities relevant to film-like and thread-like phases are discussed in § 5. The existence of an intermediate  $q$ -range where the two intensities respectively behave as  $\mathcal{P}_S/q^2$  and as  $\mathcal{P}_C/q$  is proved in § 5.1 and § 5.2. Of course, both intensities behave as  $\mathcal{P}/q^4$  in the outer  $q$ -range. The analytic expressions of pre-factors  $\mathcal{P}_S$  and  $\mathcal{P}_C$  are also worked out and three simple illustrations are reported. In § 5.3 one discusses the behavior of the scattering intensity of a right parallelepiped. If the sizes of the sides differ more than two order of magnitudes, one finds that the intensity at first behaves as  $1/q$ , then as  $1/q^2$  and finally as  $1/q^4$  in agreement with the fact that the parallelepiped looks as a thread when observed on a large scale, as a film when the observation scale becomes smaller and, finally, as a parallelepiped when the observation scale has become fine enough to resolve all the involved lengths. Section 6 draws the final conclusions.

## 2 Basic definitions and properties of the SPFs

Consider a statically isotropic sample made up of three homogeneous phases. The  $i$ th of these occupies the spatial set  $\mathcal{V}_i$ , of volume  $V_i$ , and has scattering density  $n_i$ . The total sample occupies the union set  $\mathcal{V} = \mathcal{V}_1 \cup \mathcal{V}_2 \cup \mathcal{V}_3$  of volume  $V$ . The volume fraction of the  $i$ th phase is  $\phi_i \equiv V_i/V$ . The correlation function of the sample is given by (Ciccariello and Riello, 2007)

$$\gamma(r) = \sum_{i=1}^3 \frac{n(i; j, k) \phi_i (1 - \phi_i)}{2 \langle \eta^2 \rangle} \Gamma_i(r), \quad i \neq j \neq k. \quad (1)$$

Here  $n(i; j, k)$  denotes the scattering contrast between phase  $i$  and the remaining pair of phases  $(j, k)$ . It is defined as

$$n(i; j, k) \equiv (n_i - n_j)^2 + (n_i - n_k)^2 - (n_j - n_k)^2. \quad (2)$$

$\langle \eta^2 \rangle$  is the mean square scattering density fluctuation. It is equal to  $\sum_{1 \leq i < j \leq 3} (n_i - n_j)^2 \phi_i \phi_j$  or to  $\sum_{i=1}^3 n(i; j, k) \phi_i (1 - \phi_i) / 2$ . Finally, according to the definition

$$\Gamma_i(r) \equiv \frac{P_{i,i}(r) - \phi_i^2}{\phi_i (1 - \phi_i)}, \quad i = 1, 2, 3, \quad (3)$$

$\Gamma_i(r)$  denotes the CF of the  $i$ th phase. It is determined by the only geometry of the  $i$ th phase because  $P_{i,i}(r)$  is the *stick probability function* (SPF) relevant to the phase pair  $(i, i)$ . The SPFs were first introduced by Debye *et al.* (1957) [see, also, Peterlin (1965) and Goodisman & Brumberger (1971)], in analogy with the Patterson function, according to the definition

$$P_{i,j}(r) \equiv \frac{1}{4\pi V} \int d\hat{\omega} \int_{R^3} \rho_i(\mathbf{r}_1) \rho_j(\mathbf{r}_1 + r\hat{\omega}) dv_1, \quad i, j = 1, 2, 3. \quad (4)$$

Here  $\rho_i(\mathbf{r})$  is the characteristic function of the set  $\mathcal{V}_i$  (i.e.  $\rho_i(\mathbf{r})$  is equal to one or zero depending on whether the tip of  $\mathbf{r}$  falls inside or outside  $\mathcal{V}_i$ ) and  $\hat{\omega}$  denotes a unit vector that spans all possible directions. The first integral, it being an angular average, ensures the assumed isotropy of the sample. The probabilistic meaning of the SPFs defined by (4) implies (Goodisman & Brumberger, 1971) that

$$P_{i,j}(\infty) = \phi_i \phi_j \quad \text{and} \quad P_{i,j}(0) = \phi_i \delta_{i,j}, \quad (5)$$

where  $\delta_{i,j}$  is Kronecker's symbol. Once the above equalities are substituted within equations (1) and (3) one finds that, whatever  $i$ ,

$$\gamma(0) = \Gamma_i(0) = 1 \quad \text{and} \quad \gamma(\infty) = \Gamma_i(\infty) = 0. \quad (6)$$

Definitions (1) and (3) imply that the  $r$ -dependence of the sample CF is determined by that of the SPFs that will now briefly reviewed. To this aim it is observed that the SPFs can also be written as (Ciccariello *et al.* 1981)

$$P_{i,j}(r) = \frac{1}{4\pi V} \int d\hat{\omega} \int_{\mathcal{V}_i} dv_1 \int_{\mathcal{V}_j} dv_2 \delta_3(\mathbf{r}_1 + r\hat{\omega} - \mathbf{r}_2), \quad (7)$$

where  $\delta_3(\cdot)$ , as specified by the index value, denotes the three-dimensional Dirac function. From this expression follows that the behavior of  $P_{i,i}(r)$ , as  $r \rightarrow 0$ , mainly reflects the geometrical features of surface  $\mathcal{S}_i$  that separates the  $i$ th phase from the remaining ones. In fact, it results that

$$P_{i,i}(r) \approx \mathfrak{P}_i(r) \equiv \phi_i - \frac{r S_i}{4V} + \frac{r^2 \mathfrak{A}_i}{12\pi V} + \frac{r^3}{24V} [\mathfrak{K}_i + \mathfrak{S}_i], \quad (8)$$

where  $S_i$  denotes the area of surface  $\mathcal{S}_i$  (Porod, 1951),  $L_i$  is the total length of edges  $\mathcal{L}_i$  present on  $\mathcal{S}_i$  and, finally,  $\mathfrak{A}_i$ ,  $\mathfrak{K}_i$  and  $\mathfrak{S}_i$  respectively are the *angularity* (Mering & Tchoubar, 1968; Porod, 1967; Ciccariello, 1984), the *curvosity* (Kirste & Porod, 1962) and the *sharpness* (Ciccariello & Sobry, 1995) of the  $\mathcal{S}_i$  surface. These quantities are defined as follows

$$\mathfrak{A}_i = \int_{\mathcal{L}_i} \left[ 1 + (\pi - \alpha_i(\ell)) \cot(\alpha_i(\ell)) \right] d\ell + \sum_J \frac{4\pi^2}{\mathfrak{H}_J^{1/2}}, \quad (9)$$

$$\mathfrak{K}_i = \frac{1}{2} \int_{\mathcal{S}_i} \left[ 3 H^2(\mathbf{r}) - K_G(\mathbf{r}) \right] dS \quad (10)$$

and

$$\mathfrak{S}_i = \sum_I \sum'_{i,j,\ell} (-1)_{i,j,\ell} \mathcal{V}_{i,j,\ell}(\gamma_{i,j}, \gamma_{i,\ell}, \alpha_i), \quad (11)$$

with

$$\begin{aligned}
\mathcal{V}_{i,j,\ell}(\gamma_{i,j}, \gamma_{i,\ell}, \alpha_i) = & -\frac{1}{4} \left( 1 + 2\pi (\cot \alpha_i / \sin \alpha_i) (\cot \gamma_{i,j} + \cot \gamma_{i,\ell}) + \right. \\
& (\pi - \gamma_{i,j}) [\cot \gamma_{i,j} - 2(\cot \alpha_i \cot \alpha_j) / \sin \gamma_{i,j}] + \\
& (\pi - \gamma_{i,\ell}) [\cot \gamma_{i,\ell} - 2(\cot \alpha_i \cot \alpha_\ell) / \sin \gamma_{i,\ell}] - \\
& \left. (\pi - \gamma_{j,\ell}) [\cot \gamma_{j,\ell} - 2(\cot \alpha_i \sin \gamma_{j,\ell}) / (\sin \gamma_{i,j} \sin \gamma_{i,\ell} \sin \alpha_i)] \right). \tag{12}
\end{aligned}$$

In (9), the first contribution (Ciccariello *et al.*, 1981) refers to the edges and  $\alpha_i(\ell)$  denotes the dihedral angle value at the edge point with curvilinear coordinate  $\ell$ . The second contribution (Ciccariello & Benedetti, 1982) arises from possible points of contact between different branches of surface  $\mathcal{S}_i$ . These points are indexed by  $J$ , and  $\mathfrak{H}_J$  denotes the corresponding value of the Hessian of the function resulting from the difference of the two branches. Kirste & Porod (1962) obtained equation (10). Here  $H(\mathbf{r})$  and  $K_G(\mathbf{r})$  respectively denote the mean and the Gaussian curvatures of surface  $\mathcal{S}_i$  at the point (with position vector)  $\mathbf{r}$ . The two curvatures are related to the minimum  $[R_m(\mathbf{r})]$  and the maximum  $[R_M(\mathbf{r})]$  curvature radius of the surface by

$$H(\mathbf{r}) = \frac{1}{2} \left( \frac{1}{R_m(\mathbf{r})} + \frac{1}{R_M(\mathbf{r})} \right), \tag{13}$$

$$K_G(\mathbf{r}) = \frac{1}{R_m(\mathbf{r}) R_M(\mathbf{r})}. \tag{14}$$

Finally, equation (11) was obtained by Ciccariello & Sobry (1995). The outer summation there present is performed over all the vertex points of  $\mathcal{S}_i$  and the inner one over all distinct triple of edges that enter into the  $I$ th vertex. Further,  $\gamma_{i,\ell}$  denotes the angle formed by the  $i$ th and the  $\ell$ th edge while  $\alpha_i$  is the dihedral angle at the  $i$ th edge. It is also noted that, whenever a couple of facets do not share a common edge but only a vertex, one has to consider the virtual edge along which the facets, once they are prolonged, intersect each other. This fact explains the presence in (12) of the sign factor  $(-1)_{i,j,\ell}$ . One should refer to page 65 of the above paper for the full definition. This paper also shows that the SPF of a phase bounded by a polyhedral surface is a 3rd degree polynomial within the innermost range of distances, *i.e.* it is exactly given by equation (8) with  $H = K_G = 0$ .

A further property of SPFs is the fact that, whenever parts of the interfaces are parallel to each other at a relative orthogonal distance  $\delta$ , the second derivative of the relevant SPF shows a finite (Wu & Schmidt, 1974) or a logarithmic discontinuity (Ciccariello, 1989) as  $r \rightarrow \delta$ . This property was

thoroughly discussed by Ciccariello (1991) and is practically useful (see, *e.g.*, Melnichenko & Ciccariello, 2012 and references therein). This property applies to film-like samples and yields an oscillatory contribution decreasing as  $q^{-4}$  in the range  $q > 2\pi/\delta$ . For simplicity, however, this contribution will not explicitly be considered in § 5.1.

### 3 Film-like phase and surface CF

Assume now that phase 1 have a film-like structure, *i.e.*  $\mathcal{V}_1$  is a connected or disconnected set delimited by a left ( $\mathcal{S}_{1,l}$ ) and a right ( $\mathcal{S}_{1,r}$ ) surface at a relative constant orthogonal distance  $\delta$ . Moreover, one also assumes that  $\mathcal{S}_{1,l}$  and  $\mathcal{S}_{1,r}$  be smooth (*i.e.* they have no edges, vertices and contact points) and that  $\delta$  be small in the sense that it obeys the inequality

$$\delta \ll \bar{R}_s \equiv \langle (1/R_m^2 + 1/R_M^2) \rangle^{-1/2}, \quad (15)$$

where  $\bar{R}_s$  denotes the mean value of the curvature radii of  $\mathcal{S}_1 = \mathcal{S}_{1,l} \cup \mathcal{S}_{1,r}$ , the surface bounding  $\mathcal{V}_1$ . Denote the surface midway  $\mathcal{S}_{1,l}$  and  $\mathcal{S}_{1,r}$  by  $\mathcal{S}_f$ . Then,  $\mathbf{r}_1$ , the position vector of a generic point P of  $\mathcal{V}_1$ , can uniquely be written as

$$\mathbf{r}_1 = \bar{\mathbf{r}}_1 + \xi \hat{\nu}(\bar{\mathbf{r}}_1), \quad (16)$$

where  $\bar{\mathbf{r}}_1$  denotes the position of the point intersection of  $\mathcal{S}_f$  with the straight line [with direction  $\hat{\nu}(\bar{\mathbf{r}}_1)$ ] that going through P, is normal to  $\mathcal{S}_f$ .  $\xi$  is the orthogonal distance of P from  $\mathcal{S}_f$ . In equation (7) with  $i = j = 1$ , the infinitesimal volume element  $dv_1$  located at  $\mathbf{r}_1$  can be written, up to terms  $o(\delta)$ , as [see, *e.g.*, equation (4.7) of Ciccariello (1991)]

$$dv_1 = [1 + \xi H(\bar{\mathbf{r}}_1)] dS_1 d\xi, \quad -\delta/2 \leq \xi \leq \delta/2, \quad (17)$$

where  $dS_1$  is the infinitesimal surface element of  $\mathcal{S}_f$  located at  $\bar{\mathbf{r}}_1$ . Using equations (16), (17) and (7), one concludes that the SPF of film-like phase 1 takes the form

$$P_{1,1}(r) \equiv \frac{1}{4\pi V} \int_{-\delta/2}^{\delta/2} d\xi_1 \int_{-\delta/2}^{\delta/2} d\xi_2 \int d\hat{\omega} \int_{\mathcal{S}_f} dS_1 \int_{\mathcal{S}_f} dS_2 (1 + \xi_1 H(\bar{\mathbf{r}}_1)) \times \\ (1 + \xi_2 H(\bar{\mathbf{r}}_2)) \delta_3(\bar{\mathbf{r}}_1 + \xi_1 \hat{\nu}(\bar{\mathbf{r}}_1) + r\hat{\omega} - \bar{\mathbf{r}}_2 - \xi_2 \hat{\nu}(\bar{\mathbf{r}}_2)). \quad (18)$$

### 3.1 The surface CF definition

In the range of distances  $0 \leq r < \delta$  this function is reliably approximated by equation (8) that in the present case reads

$$P_{1,1}(r) \approx \mathfrak{P}_{1,S}(r) \equiv \phi_i - \frac{2S_f r}{4V} + \frac{r^3 S_f}{48V} \left( \langle 3H^2 - K_G \rangle_{S_f} \right) \quad \text{if } 0 < r < \delta, \quad (19)$$

since the smoothness of the surface and the smallness of  $\delta$  makes the surface area approximation  $S_1 \approx 2S_f$  accurate.

In the range  $r > \delta$ , the smallness of  $\delta$  makes it possible to set  $\xi_1 = \xi_2 = 0$  within the integrand of (18) so that the SPF becomes

$$P_{1,1}(r) \approx \frac{\delta^2 S_f}{V} \gamma_S(r) \quad \text{if } r > \delta, \quad (20)$$

with

$$\gamma_S(r) \equiv \frac{1}{4\pi S_f} \int d\hat{\omega} \int_{S_f} dS_1 \int_{S_f} dS_2 \delta_3(\bar{\mathbf{r}}_1 + r\hat{\omega} - \bar{\mathbf{r}}_2), \quad r > 0. \quad (21)$$

Function  $\gamma_S(r)$  is named *surface correlation function* because it is fully determined by the surface set  $S_f$ . Function  $\gamma_S(r)$  was first introduced by Teubner (1990). [Note, however, that this author used  $\frac{1}{4\pi V}$ , instead of  $\frac{1}{4\pi S_f}$ , as normalization factor in front of the integral reported in (21).]

Figures 1 and 2 show the accuracy achieved in approximating the bulk SPF  $P_{1,1}r$  by the 3rd degree  $r$ -polynomial (19) in the range  $0 < r < \delta$  and by the surface CF, via equation (20), in the range  $r > \delta$  for two simple particle shapes: the spherical shell and the cylindrical disk. The accuracy drastically improves as  $\delta$  gets smaller.

### 3.2 Properties of the surface CF

From equation (20) and the fact that  $P_{1,1}(r)$  is dimensionless it follows that the surface CF has dimension  $\text{length}^{-1}$ . The leading behavior of the surface CF as  $r \rightarrow 0$  was obtained by Teubner (1990), under the assumption that the surface is closed [*i.e.*, with no boundary] and smooth, by the same procedure that Kirste & Porod (1962) followed to get their relation. It reads

$$\gamma_S(r) \approx \frac{1}{2r} + \frac{r}{32} \left\langle \left( \frac{1}{R_m} - \frac{1}{R_M} \right)^2 \right\rangle + o(r), \quad (22)$$

where the angular brackets denote the average over  $S_f$ . This relation shows that the surface CF diverges as  $r \rightarrow 0$  so that it cannot be normalized to one



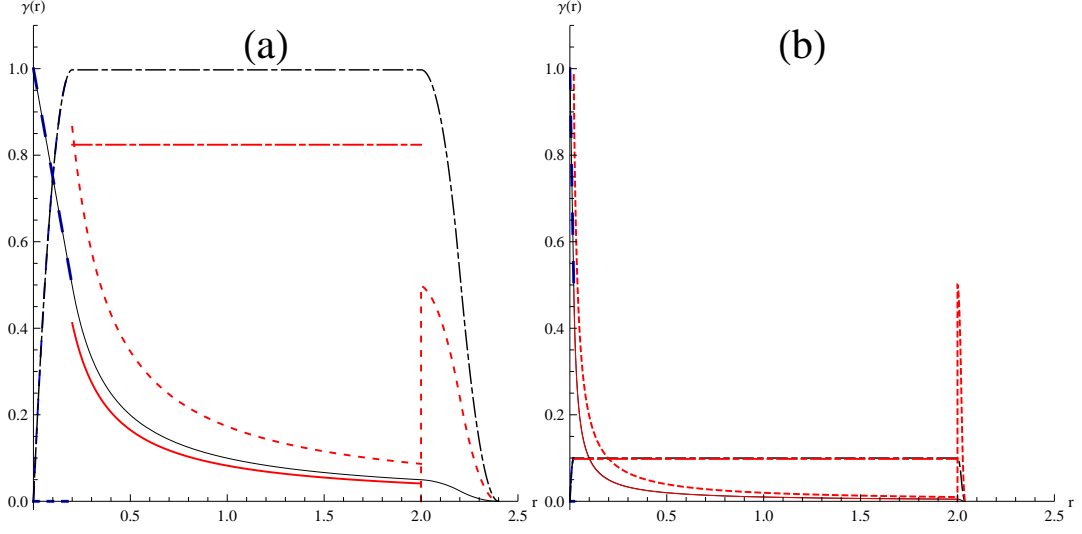


Figure 1: (a): the black continuous line plots  $\gamma_{\mathcal{V},ss}(r)$ , the CF of a spherical shell [it is recalled that in the case of a single particle one has  $\phi_1 = 1$  and  $P_{1,1}(r) = \gamma_{\mathcal{V},ss}(r)$ , the last function being given by (40)] with inner and outer radii equal to  $R_i = R = 1$  and  $R_o = 1.2$ , so that  $\delta = (R_o - R_i) = 0.2$  and  $\delta/\bar{R} = 0.25$ . [For the  $\bar{R}$  definition see equation (15)]. The continuous red line is the plot of  $\delta^2 S_f \gamma_{\mathcal{S},sph}(r, R)/V$  within the range  $\delta < r < 2R$ ,  $\gamma_{\mathcal{S},sph}(r, R)$  being the CF of a spherical surface of radius  $R = 1$  [see equation (41)]. The thick long-dash blue curve is the plot of  $\mathfrak{P}_{1,S}(r)$ . The dotted blue (hardly visible) and red curves show the approximation discrepancy since they plots  $c \cdot (\gamma_{\mathcal{V},ss}(r) - \mathfrak{P}_{1,S}(r))$  and  $c \cdot (\gamma_{\mathcal{V},ss}(r) - \delta^2 S_f \gamma_{\mathcal{S},sph}(r, R)/V)$  with  $c = 10$ . The dash-dotted black, blue and red broken lines respectively are the plots  $10 \cdot r \gamma_{\mathcal{V},ss}(r)$ ,  $10 \cdot r \mathfrak{P}_{1,S}(r)$  and  $10 \cdot r \delta^2 S_f \gamma_{\mathcal{S},sph}(r, R)/V$  (red). (b): as in (a) with  $R_i = 1$  and  $\delta = 0.02$  and  $c = 100$  (the dash-dotted curves merge in the single red one). The two panels makes it evident that the approximation gets more and more accurate as  $\delta/R$  decreases.

at the origin as it happens for standard CFs.

As  $r \rightarrow \infty$ , the leading behavior of the surface CF is

$$\gamma_S(r) \approx \frac{S_f}{V}. \quad (23)$$

This immediately follows from equations (5) and (20) since

$$\lim_{r \rightarrow \infty} \gamma_S(r) = \lim_{r \rightarrow \infty} \frac{V}{\delta^2 S_f} P_{1,1}(r) \approx \frac{V \phi_1^2}{\delta^2 S_f} \approx \frac{V S_f^2 \delta^2}{\delta^2 S_f V^2} = \frac{S_f}{V}.$$

It is also noted that the surface CF defined by equation (21) generalizes the two dimensional (2D) CF defined as (Ciccariello, 2009)

$$\gamma_2(r) = \frac{1}{2\pi S} \int d\hat{\omega} \int_S dS_1 \int_S dS_2 \delta_2(\mathbf{r}_1 + r\hat{\omega} - \mathbf{r}_2), \quad (24)$$

where  $\mathcal{S}$  is a plane set and  $\hat{\omega}$  is a unit vector that spans the unit circle. To get the relation between the two quantities in the case where the  $\mathcal{S}_f$  set, present in (21), is plane, one chooses the plane where  $\mathcal{S}_f$  lies as the  $z = 0$  plane. Then, in (21) one writes

$$\delta_3(\mathbf{r}_1 + r\hat{\omega} - \mathbf{r}_2)d\hat{\omega} = \delta_2(\mathbf{r}_1 + r\hat{\omega}_{||} - \mathbf{r}_2)\delta_1(r\cos\theta)d\varphi d(\cos\theta),$$

[where  $\hat{\omega}_{||}$  is the projection of  $\hat{\omega}$  onto the  $z = 0$  plane] and, after integrating over  $\theta$ , one gets

$$\gamma_S(r) = \frac{1}{4\pi S_f r} \int d\hat{\omega} \int_{S_f} dS_1 \int_{S_f} dS_2 \delta_2(\mathbf{r}_1 + r\hat{\omega} - \mathbf{r}_2), \quad (25)$$

where the outermost integral is performed on the unit circle. Comparing (25) with (24) and assuming that  $\mathcal{S}_f = \mathcal{S}$  one finds

$$2r\gamma_S(r) = \gamma_2(r). \quad (26)$$

Ciccariello (2010) showed that, as  $r \rightarrow 0$ ,  $\gamma_2(r) \approx (1 - rL/\pi S)$  where  $L$  denotes the length of the boundary of  $\mathcal{S}$ . Thus, relation (26), allows us to generalize equation (22) to the case where  $\mathcal{S}_f$  is an open surface, and has therefore a boundary of perimeter  $L_f$ , in the following way

$$\gamma_S(r) \approx \frac{1}{2r} - \frac{L_f}{2\pi S_f} + \frac{r}{32} \left\langle \left( \frac{1}{R_m} - \frac{1}{R_M} \right)^2 \right\rangle + o(r) \quad \text{as } r \rightarrow 0. \quad (27)$$

Finally it is observed that the moments of the surface CF can be expressed in terms of the moments of the surface if  $\frac{S_f}{V} \approx 0$ . In fact, putting

$$M_{S,m} \equiv \int_0^\infty r^{2m+2} \gamma_S(r) dr, \quad (28)$$

from equation(21) follows

$$\begin{aligned} M_{S,m} &= \frac{1}{4\pi S_f} \int r^{2m} dv \int_{S_f} dS_1 \int_{S_f} dS_2 \delta_3(\bar{\mathbf{r}}_1 + \mathbf{r} - \bar{\mathbf{r}}_2) \\ &= \frac{1}{4\pi S_f} \int_{S_f} dS_1 \int_{S_f} dS_2 (\mathbf{r}_2 - \mathbf{r}_1)^{2m}. \end{aligned} \quad (29)$$

The last expression is equal to the sum of products of different moments of surface  $\mathcal{S}_f$  [see appendix B of Ciccariello (2014)]. In particular, if  $m = 0$ , one simply finds

$$M_{S,0} = \frac{S_f}{4\pi}. \quad (30)$$

### 3.3 Integral expressions of the derivatives of the surface CF

The comparison of (21) with equation (3.1) of Ciccariello *et al.* (1981) shows that the surface CF and the second derivative of  $P_{1,1}(r)$  nearly have the same mathematical structure since the only difference, aside from the normalization factors, lies in the angular contribution  $(\hat{\nu}(\bar{\mathbf{r}}_1) \cdot \hat{\omega})(\hat{\nu}(\bar{\mathbf{r}}_2) \cdot \hat{\omega})$  that is only present in the  $P_{1,1}''(r)$  expression. Consequently, many of the elaborations worked out for this expression apply, *mutatis mutandis*, to the surface CF. In particular, let  $\Sigma(\mathbf{r}_1, r)$  denote the spherical surface with center at  $\mathbf{r}_1$  and radius  $r$ . Then equation (21) can be written as

$$\gamma_S(r) = \frac{1}{4\pi S_f r^2} \int_{S_f} dS_1 \int_{\Sigma(\bar{\mathbf{r}}_1, r)} dS \int_{S_f} \delta_3(\bar{\mathbf{r}}_1 + r\hat{\omega} - \bar{\mathbf{r}}_2) dS_2. \quad (31)$$

Omitting the overbar, denoting by  $\mathcal{C}_\Sigma(\mathbf{r}_1, r)$  the intersection curve of  $\Sigma(\mathbf{r}_1, r)$  with  $S_f$  (it is formed by the points of  $S_1$  that are at distance  $r$  from point  $\mathbf{r}_1$  of  $S_f$ ) and proceeding as in the just mentioned paper, one finds that  $\gamma_S(r)$  takes the form

$$\gamma_S(r) = \frac{1}{4\pi S_f r^2} \int_{S_f} dS_1 \int_{\mathcal{C}_\Sigma(\bar{\mathbf{r}}_1, r)} \frac{1}{\sqrt{1 - (\hat{\nu}(\mathbf{r}_1 + r\hat{\omega}(\ell)) \cdot \hat{\omega}(\ell))^2}} d\ell. \quad (32)$$

In this expression,  $\ell$  is the curvilinear coordinate of the curve points (note that the curvilinear coordinate definition is such that the distance between two points, having curvilinear coordinates  $\ell$  and  $\ell + d\ell$ , is equal to  $d\ell$ ),  $\hat{\nu}(\mathbf{r}_1 + r\hat{\omega}(\ell))$  denotes the unit vector orthogonal to (and pointing outwardly to)  $S_f$  at the point  $\mathbf{r}_2(\ell) \equiv \mathbf{r}_1 + r\hat{\omega}(\ell)$  and  $\hat{\omega}(\ell)$  specifies the direction of the vector  $(\mathbf{r}_2(\ell) - \mathbf{r}_1)$ .

If one puts

$$\cos \Theta(\mathbf{r}_1, r, \ell) \equiv \hat{\nu}(\mathbf{r}_1 + r\hat{\omega}(\ell)) \cdot \hat{\omega}(\ell), \quad (33)$$

and

$$p(\mathbf{r}_1, r) \equiv \int_{\mathcal{C}_\Sigma(\mathbf{r}_1, r)} \frac{1}{r^2 \sin \Theta(\mathbf{r}_1, r, \ell)} d\ell, \quad (34)$$

equation (32) becomes

$$\gamma_S(r) = \frac{1}{4\pi S_f} \int_{S_f} dS_1 \int_{\mathcal{C}_\Sigma(\mathbf{r}_1, r)} \frac{1}{r^2 \sin \Theta(\mathbf{r}_1, r, \ell)} d\ell = \frac{1}{4\pi S_f} \langle p(\cdot, r) \rangle_{S_f}. \quad (35)$$

Thus,  $\gamma_S(r)$  is proportional to  $\langle p(\cdot, r) \rangle_{S_f}$  that denotes the average value of  $p(\mathbf{r}_1, r)$  over  $S_f$ . The  $n$ th derivative of  $\gamma_S(r)$  takes the form

$$\gamma_S^{(n)}(r) = \frac{1}{4\pi S_f} \int d\hat{\omega} \int_{S_f} dS_1 \int_{S_f} dS_2 (-\hat{\omega} \cdot \nabla_2)^n \delta(\bar{\mathbf{r}}_1 + r\hat{\omega} - \bar{\mathbf{r}}_2), \quad (36)$$

which implies that the reduced integral expressions involve an integration, along the same  $\mathcal{C}_\Sigma(\mathbf{r}_1, r)$  curve, of an integrand that changes with the derivative order  $n$ . To get the integrand expression, proceeding as in Ciccariello (1995), one denotes by  $\mathbf{R}(u, v)$  the parametric equation of  $\mathcal{S}_1$ , and by  $\mathbf{R}_u(u, v)$  and  $\mathbf{R}_v(u, v)$  the corresponding derivatives with respect to  $u$  and  $v$ . One puts

$$\vec{\mathcal{A}}^{(0)}(\mathbf{r}_1, \mathbf{r}_2(\ell), r) \equiv \frac{\hat{\tau}(\ell)}{\|\mathbf{R}(u(\ell), v(\ell)) - \mathbf{r}_1\|^2 \sin \Theta(\mathbf{r}_1, r, \ell)}, \quad (37)$$

[where  $\mathbf{r}_2(\ell) \equiv \mathbf{R}(u(\ell), v(\ell))$  and  $\hat{\tau}(\ell)$  denotes the unit vector tangent to  $\mathcal{C}_\Sigma(\mathbf{r}_1, r)$  at  $\mathbf{r}_2(\ell)$ ] and

$$\vec{\mathcal{A}}^{(n)}(\mathbf{r}_1, \mathbf{r}_2(\ell), r) \equiv \frac{\mathbf{R}_u \cdot \vec{\mathcal{A}}_v^{(n-1)} - \mathbf{R}_v \cdot \vec{\mathcal{A}}_u^{(n-1)}}{\|\mathbf{R}_u \times \mathbf{R}_v\| \sin \Theta(\mathbf{r}_1, r, \ell)} \hat{\tau}(\ell), \quad n = 1, 2, \dots \quad (38)$$

where the reported partial derivatives are evaluated at the argument values shown on the left hand side. In this way, the integral expression of the  $n$ th derivative of the surface CF becomes

$$\gamma_{\mathcal{S}}^{(n)}(r) = \frac{1}{4\pi S_f} \int_{\mathcal{S}_f} dS_1 \int_{\mathcal{C}_\Sigma(\mathbf{r}_1, r)} \left( \vec{\mathcal{A}}^{(n)}(\mathbf{r}_1, \mathbf{r}_2(\ell), r) \cdot \hat{\tau}(\ell) \right) d\ell \quad (39)$$

under the assumption that the involved partial derivatives exist.

### 3.4 Examples of surface CFs

The following subsections report the surface CFs relevant to a spherical surface, a circle and a rectangle, while the surface CF of a cubic surface is worked out in appendix B.

#### 3.4.1 The CF of spherical surface

Consider a spherical shell of inner and outer radius equal to  $R$  and  $R + \delta$  with  $\delta < R$ . The bulk CF was calculated by Glatter (1982) (see also Fedorova & Emelyanov, 1977) and reads

$$\gamma_{\mathcal{V},ss}(r) = \begin{cases} \frac{\pi(r^3 - 6r(2R^2 + 2R\delta + \delta^2) + 8\delta(3R^2 + 3R\delta + \delta^2))}{6V} & \text{if } 0 < r < \delta, \\ \frac{\pi\delta^2(2R + \delta)^2}{2rV} & \text{if } \delta < r < 2R, \\ \frac{\pi(12r^2R^2 - r^4 - 16rR^3 + 6\delta^2(2R + \delta)^2)}{12rV} & \text{if } 2R < r < 2R + \delta, \\ \frac{\pi(r - 2(R + \delta))^2(r + 4(R + \delta))}{12V} & \text{if } 2R + \delta < r < 2R + 2\delta, \\ 0 & \text{if } 2R + 2\delta < r, \end{cases} \quad (40)$$

with  $V = 4\pi((R + \delta)^3 - R^3)/3$ .

As  $\delta \rightarrow 0$ , the spherical shell becomes a spherical surface of radius  $R$ . The corresponding CF is easily evaluated by (35). In fact,  $\mathcal{C}_\Sigma(\mathbf{r}_1, r)$  is a circle of radius  $R_1 = r \sqrt{1 - r^2/4R^2}$  and  $\cos \Theta(\mathbf{r}_1, r, \ell) = r/2R$ . In this way, from (35) follows that

$$\gamma_{S, sph}(r, R) = \begin{cases} \frac{1}{2r} & \text{if } 0 < r < 2R, \\ 0 & \text{if } 2R < r. \end{cases} \quad (41)$$

This expression is equal to  $\lim_{\delta \rightarrow 0} V\gamma_{V, ss}(r)/S_f\delta^2$  as required by equation (20). Figures 1a and 1b allows one to appreciate the accuracy achievable in approximating  $\gamma_{V, ss}(r)$  by  $\delta^2 S_f\gamma_{S, sph}(r, R)/V$  for the cases  $(R, \delta) = (1, 0.2)\text{u}$  and  $(1, 0.02)\text{u}$ , respectively.

### 3.4.2 The surface CF of a circle

Consider a circular cylinder of radius  $R$  and height  $h$ . If one lets  $h$  go to zero, the cylinder shrinks to a circle of radius  $R$ . The surface CF of the circle is easily evaluated by equation (26). In fact the value of the 2D CF of a circle at a given distance  $r$  is proportional to the overlapping area of the outset circle and the circle shifted by  $r$ . In this way, accounting for the appropriate proportionality constant, one finds that the surface CF  $\gamma_{S, crcl}(r, R)$  of a circle is

$$\gamma_{S, crcl}(r, R) = \begin{cases} -\frac{\sqrt{4R^2 - r^2}}{4\pi R^2} + \frac{1}{\pi r} \arccos \frac{r}{2R} & \text{if } 0 < r < 2R, \\ 0 & \text{if } 2R < r. \end{cases} \quad (42)$$

One easily verifies that

$$\lim_{h \rightarrow 0} \frac{V_{cyl}}{h^2 S_f} \gamma_{dsk}(r, R, h) = \gamma_{S, crcl}(r, R),$$

where  $\gamma_{dsk}(r, R, h)$  denotes the cylinder CF that is given by (108). Besides, the small distance expansion of (42) yields

$$\gamma_{S, crcl}(r, R) \approx \frac{1}{2r} - \frac{1}{\pi R} + \frac{r^2}{24\pi R^3} + O(r^3), \quad (43)$$

in agreement with equation (27).

Similarly to Fig. 1, Fig. 2 shows the accuracy achieved in approximating  $\gamma_{dsk}(r, R, h)$ , the cylinder CF, by the relevant  $\mathfrak{P}_{1, S}(r)$  polynomial within the range  $0 < r < h$  and by  $h^2 S_f \gamma_{S, crcl}(r, R)/V_{cyl}$  if  $r > h$  in the case where the cylinder has height equal to  $h = 0.2\text{u}$  and radius equal to  $R = 1\text{u}$ .

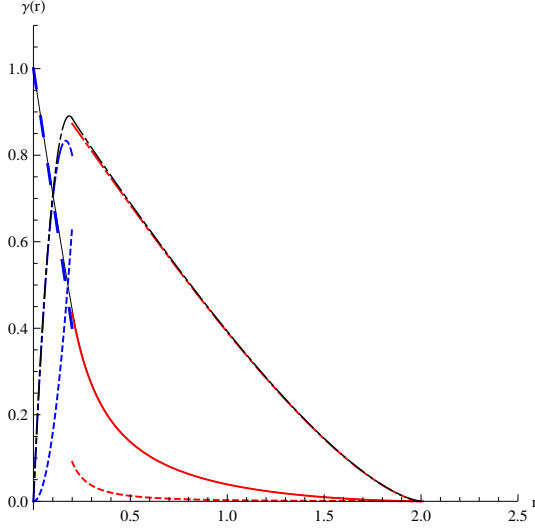


Figure 2: The shown curves have the same meaning of those reported in Fig. 1. They do however refer to a circular cylinder of radius  $R = 1u$  and height  $h = 0.2u$ . The black, blue and red dash-dotted curves are the plots of  $10 \cdot r \gamma_{dsk}(r, R, h)$  [see equation(108)],  $10 \cdot r \mathfrak{P}_{1,S}(r)$  [see Eq. (19)] and  $10 \cdot r h^2 S_f \gamma_{S,crcl}(r, R)/V_{cyl}$  [see Eq. (42)]. The dotted curves plot the approximation error multiplied by  $c = 15$ .

### 3.4.3 The surface CF of a rectangle

Consider a rectangle of sides  $a$  and  $b$  with  $a < b$ . Its surface CF  $\gamma_{S,rect}(r, a, b)$  is easily obtained using equation (26) and recalling that the 2D CF of any plane polygon has an algebraic form (Ciccariello, 2009). Hence, using the result of this paper, one finds that the surface CF of the aforesaid rectangle is

$$\gamma_{S,rect}(r; a, b) = \begin{cases} \frac{\pi ab - 2(a+b)r + r^2}{2\pi rab}, & 0 < r < a, \\ -\frac{a^2 + 2br - 2b\sqrt{r^2 - a^2} - 2ab \arcsin(a/r)}{2\pi rab}, & a < r < b, \\ -\frac{a^2 + b^2 + r^2 - 2b\sqrt{r^2 - a^2} - 2a\sqrt{r^2 - b^2}}{2\pi rab} - \frac{2ab(\arccos(b/r) - \arcsin(a/r))}{2\pi rab}, & b < r < \sqrt{a^2 + b^2}, \\ 0, & \sqrt{a^2 + b^2} < r. \end{cases} \quad (44)$$

## 4 Thread-like phase and curve CF

Consider now the case where one of the sample phases (named again phase 1) is formed by threads having the same normal section of maximal chord  $2\delta$

and area  $\sigma$ . Assume that  $\delta$  be small (in a sense that will be defined later). Then, in the limit  $\sigma \rightarrow 0$ , phase 1 shrinks to a curve  $\mathcal{C}$  that might have branching points. The number of these points is assumed to be negligible. The curve  $\mathcal{C}$  can be parameterized as

$$\mathbf{R} = \mathbf{R}(\ell) = (X(\ell), Y(\ell), Z(\ell)), \quad (45)$$

where  $\ell$  denotes the curvilinear coordinate of the curve point set at  $\mathbf{R}$ . It is also assumed that  $\mathcal{C}$  is *smooth* in the sense that  $\mathbf{R}(\ell)$  is continuously differentiable up to the third order (included). Then, the curve at each of its points is endowed of two curvature radii:  $R_c(\ell)$  and  $R_t(\ell)$ , respectively named *curvature* radius and *torsion* radius (Smirnov, 1970). To define these, one considers the three mutually orthogonal unit vectors defined as follows

$$\hat{\tau}(\ell) \equiv \frac{d\mathbf{R}(\ell)}{d\ell}, \quad \hat{\mathbf{n}}(\ell) \equiv \frac{d\hat{\tau}(\ell)}{d\ell} / \left| \frac{d\hat{\tau}(\ell)}{d\ell} \right| \quad \text{and} \quad \hat{\mathbf{b}}(\ell) \equiv \hat{\tau}(\ell) \times \hat{\mathbf{n}}(\ell), \quad (46)$$

and respectively named *tangent*, *normal* and *binormal* vectors. Clearly,  $\hat{\tau}(\ell)$  specifies the direction of the tangent to  $\mathcal{C}$  at  $\mathbf{R}(\ell)$ ,  $\hat{\mathbf{n}}(\ell)$  is the unit vector orthogonal to  $\hat{\tau}(\ell)$  such that these two vectors determine the plane osculating the curve at  $\mathbf{R}(\ell)$ . Besides, the orientation of  $\hat{\mathbf{n}}(\ell)$  is such that the curve looks concave at the considered point. The expressions of the aforesaid radii are as follows

$$R_c(\ell) \equiv 1 / \left| \frac{d\hat{\tau}(\ell)}{d\ell} \right| \quad \text{and} \quad R_t(\ell) \equiv 1 / \left( \frac{d\hat{\mathbf{b}}(\ell)}{d\ell} \cdot \hat{\mathbf{n}}(\ell) \right). \quad (47)$$

The curvature radius is the radius of the circumference osculating the curve while the torsion radius specifies how the osculating plane rotates as one moves along the curve. It follows that the curvature radius is always positive while the torsion radius can be positive at some points of the curve and negative at others.

Similarly to equation (15) one defines the mean of the curvature radii of the curve as

$$\bar{R}_c \equiv \langle (1/R_c^2 + 1/R_t^2) \rangle_{\mathcal{C}}^{-1/2}, \quad (48)$$

where the average is performed integrating all over the length of  $\mathcal{C}$ . (It is noted that  $\mathcal{C}$  generally consists of many disjoint closed and/or open curves.) One goes now back to  $P_{1,1}(r)$ , the SPF of the thread-like phase, to analyze in more detail the limit  $\sigma \rightarrow 0$ . First, it is observed that  $\sigma$  is small if  $\delta \ll \bar{R}_c$  as it will hereafter be assumed. Let  $\mathbf{r}$  be the position vector of a point of phase 1 and consider the plane that contains this point and is orthogonal to  $\mathcal{C}$ . Denote respectively by  $\mathbf{R}(\ell)$  and by  $\underline{\sigma}(\ell)$  the intersections of the plane with

$\mathcal{C}$  and with the thread-like phase. One can then write  $\mathbf{r} = \mathbf{R}(\ell) + \vec{\xi}_\perp$  where  $\vec{\xi}_\perp$  lies within  $\underline{\sigma}(\ell)$ , the normal section set of the thread at  $\mathbf{R}(\ell)$ . Function  $P_{1,1}(r)$  can be written as

$$P_{1,1}(r) = \frac{1}{4\pi V} \int_{\mathcal{C}} d\ell_1 \int_{\underline{\sigma}(\ell_1)} d^2 \vec{\xi}_{1,\perp} \int_{\mathcal{C}} d\ell_2 \int_{\underline{\sigma}(\ell_2)} d^2 \vec{\xi}_{2,\perp} \times \quad (49)$$

$$\int d\hat{\omega} \delta_3(\mathbf{R}(\ell_1) + \vec{\xi}_{1,\perp} + r\hat{\omega} - \mathbf{R}(\ell_2) - \vec{\xi}_{2,\perp}).$$

The volume fraction of the thread-like phase is fairly approximated by  $\phi_1 = \sigma L/V$  with  $L$  equal to the total length of the threads. From equation (5) follows that

$$P_{1,1}(0) = \sigma L/V, \quad \text{and} \quad P_{1,1}(\infty) = \sigma^2(L/V)^2. \quad (50)$$

Similarly to the case discussed in § 3.1, in the range  $0 < r < 2\delta$ ,  $P_{1,1}(r)$  is fairly approximated by equation (19). This can be written in the algebraic form

$$P_{1,1}(r) \approx \mathfrak{P}_{1,c}(r) \equiv \frac{\sigma L}{V} - \frac{r \pi \delta L}{2V} + \frac{\pi r^3 L}{64 V \delta}, \quad r < 2\delta, \quad (51)$$

if one approximates the threads by circular cylinders so that  $S \approx 2\pi\delta L$ ,  $H \approx \frac{1}{2\delta}$  and  $K_G \approx 0$ .

In the range  $r > 2\delta$ , owing to the smallness of  $\delta$ , one can neglect the dependence on  $\vec{\xi}_{1,\perp}$  and  $\vec{\xi}_{2,\perp}$  within the Dirac function. Then, the integrals over these variables can explicitly be performed and one finds that

$$P_{1,1}(r) \approx \frac{\sigma^2 L}{V} \gamma_{\mathcal{C}}(r), \quad r > 2\delta, \quad (52)$$

with

$$\gamma_{\mathcal{C}}(r) \equiv \frac{1}{4\pi L} \int d\hat{\omega} \int_{\mathcal{C}} d\ell_1 \int_{\mathcal{C}} d\ell_2 \delta_3(\mathbf{R}(\ell_1) + r\hat{\omega} - \mathbf{R}(\ell_2)), \quad r > 0. \quad (53)$$

One concludes that the  $r$ -dependence of the SPF of a thread-like phase is described by function  $\gamma_{\mathcal{C}}(r)$  in the outer distance range and by equation (51) in the inner one.

Function  $\gamma_{\mathcal{C}}(r)$  is determined by curve  $\mathcal{C}$  and will be named *curve correlation function*. The dimensions of  $\gamma_{\mathcal{C}}(r)$  are  $\text{length}^{-2}$ .

First one elaborates equation (53) so as to convert it into a one dimensional integral. To this aim, the equation is written as

$$\gamma_{\mathcal{C}}(r) = \frac{1}{4\pi L r^2} \int_{\mathcal{C}} d\ell_1 \int_{\Sigma(\mathbf{R}(\ell_1), r)} dS \int_{\mathcal{C}} d\ell_2 \delta(\mathbf{R}(\ell_1) + \mathbf{R} - \mathbf{R}(\ell_2)), \quad (54)$$



where  $\mathbf{R}$  denotes the position vector of the infinitesimal surface element  $dS$  of  $\Sigma(\mathbf{R}(\ell_1), r)$ , the sphere of radius  $r$  centered at the infinitesimal curve element  $d\ell_1$  set at  $\mathbf{R}(\ell_1)$ . Note that the modulus of  $\mathbf{R}$  is  $r$ . One denotes the function defined by the innermost two integrals of (54) as

$$p_C(\ell_1, r) \equiv \int_{\Sigma(\mathbf{R}(\ell_1), r)} dS \int_C d\ell_2 \delta(\mathbf{R}(\ell_1) + \mathbf{R} - \mathbf{R}(\ell_2)). \quad (55)$$

The function can easily be evaluated choosing a Cartesian orthogonal frame having the origin  $O$  at the position of  $d\ell_1$  so that  $\mathbf{R}(\ell_1) = \mathbf{0}$ . The value of the integral can be different from zero if and only if  $\Sigma(\mathbf{0}, r)$  intersects  $\mathcal{C}$ . Assume that the intersection points exist and let  $P$  denotes one of these points. Then, one chooses the  $Z$  axis along  $OP$ . The plane containing  $dS$  is perpendicular to  $Z$  while  $d\ell_2$  forms an angle, denoted by  $\theta$ , with axis  $Z$ , so that  $dZ = \cos(\theta)d\ell_2$ . Around  $P$ ,  $p_C(\ell_1, r)$  takes the form  $\int dX \int dY \int (dZ/\cos\theta) \delta_1(X) \delta_1(Y) \delta_1(Z)$  and its value is  $1/\cos(\theta)$ . Recalling that  $d\ell_2$  is parallel to  $\hat{\tau}(\ell_2)$ , with  $\hat{\tau}$  defined by equation (46a), one gets

$$\hat{\omega}(\ell_1, r) = (\mathbf{R}(\bar{\ell}_2) - \mathbf{R}(\ell_1))/r, \quad (56)$$

$$\cos(\theta(\ell_1, r)) = \hat{\omega}(\ell_1, r) \cdot \hat{\tau}(\bar{\ell}_2), \quad (57)$$

and

$$p_C(\ell_1, r) = \sum_i \frac{1}{\hat{\omega}_i(\ell_1, r) \cdot \hat{\tau}_i(\bar{\ell}_2)} = \sum_i \frac{1}{\cos(\theta_i(\ell_1, r))}, \quad (58)$$

where index  $i$  labels all the points of  $\mathcal{C}$  that are at distance  $r$  from the point set at  $\mathbf{R}(\ell_1)$ . It is stressed that equation (56) determines the direction of  $\hat{\omega}$  as well as the curvilinear coordinate value  $\ell_2$  (denoted by  $\bar{\ell}_2$ ) owing to the fact that the vector on the right side of (56) must be unimodular. By (54) and (58) one concludes that the curve CF is proportional to the curvilinear average of  $1/\cos\theta(\ell_1, r)$ , *i.e.*

$$\gamma_C(r) = \frac{1}{4\pi r^2} \left\langle \frac{1}{\cos\theta(., r)} \right\rangle_C. \quad (59)$$

The leading asymptotic behavior of the above expression as  $r \rightarrow 0$  is worked out in appendix C and reads

$$\gamma_C(r) \approx \frac{1}{2\pi r^2} + \frac{1}{16\pi} \left\langle \frac{1}{R_C^2} \right\rangle_C + o(r^2), \quad r \approx 0. \quad (60)$$

This result shows that the curve CF diverges as  $1/r^2$  as one approaches the origin. The leading behavior of the curve CF as  $r \rightarrow \infty$  is immediately obtained by equations (52) and (50b) and reads

$$\gamma_C(r) \approx L/V + O(1/r), \quad r \rightarrow \infty. \quad (61)$$

The moments  $M_{C,m}$  of the curve CF, similarly to the case of the surface CF, can be expressed in terms of the moments of the curve. In fact

$$M_{C,m} \equiv \int_0^\infty r^{2m+2} \gamma_C(r) dr = \frac{1}{4\pi L} \int_C d\ell_1 \int_C d\ell_2 (\mathbf{R}(\ell_2) - \mathbf{R}(\ell_1))^{2m}. \quad (62)$$

From this relation follows that  $M_{C,0} = L/4\pi$ .

## 4.1 Examples of curve CFs

Two examples of curve CFs are reported in the following subsections.

### 4.1.1 The curve CF of a linear segment

The first refers to a linear segment of length  $L$ . Applying definition (54), the angle defined by (57) is equal to zero. Thus, equation (59) yields

$$\gamma_{C,ls}(r, L) = \begin{cases} \frac{1}{2\pi r^2} - \frac{1}{2\pi Lr} & \text{if } 0 < r < L, \\ 0 & \text{if } L < r. \end{cases} \quad (63)$$

By letting the radius of a circular cylinder go to zero, the limit of its CF [multiplied by  $V/L\sigma^2$  as required by (52)] must reproduce (63). One easily checks that this property holds true evaluating the aforesaid limit stemming from  $\gamma_{ndl}(r, R, h)$ , the cylinder CF given by equation (109). Besides this CF can be approximated by (51) if  $r < 2R$  and by  $(\pi R^2)\gamma_{C,ls}(r, h)$  if  $r > 2R$ . Fig. 3 shows the achieved accuracy in the case  $R = \frac{1}{20}u$  and  $h = 1u$ .

### 4.1.2 The curve CF of a circumference

The curve CF of a circumference of radius  $R$  also can easily be evaluated. One puts  $\ell = R\varphi$ . Given  $r$ , the associated  $\varphi$  value is  $\varphi = \arccos((2R^2 - r^2)/2R^2)$ . Then one finds that  $\theta(\ell, r) = \pi/2 - (\pi - \varphi)/2$  so that  $\cos \theta(\ell, r) = \frac{\sqrt{4R^2 - r^2}}{2R}$ . Finally, from (59), one gets the circumference CF

$$\gamma_{C,crc}(r) = \begin{cases} \frac{R}{\pi r^2 \sqrt{4R^2 - r^2}} & \text{if } 0 < r < 2R, \\ 0 & \text{if } 2R < r. \end{cases} \quad (64)$$

This CF behaves as  $1/2\pi r^2$  as  $r \rightarrow 0$  and diverges as  $1/[2\pi R^{3/2}(2R - r)^{1/2}]$  as  $r \rightarrow 2R^-$ .

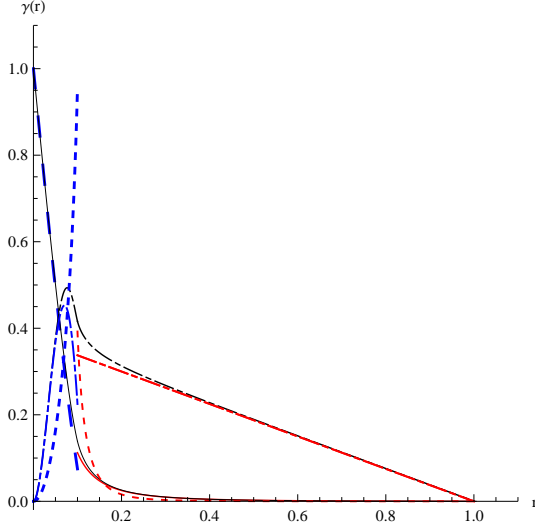


Figure 3: The curves have the same meaning as in Fig. 2. They do however refer to a circular cylinder of radius  $R = \frac{1}{20}u$  and height  $h = 1u$ . The black, blue and red dash-dotted curves are the plots of  $300 \cdot r^2 \gamma_{ndl}(r)$  [see Eq. (109)],  $300 \cdot r^2 \mathfrak{P}_{1,c}(r)$  [see Eq. (51)] and  $300 \cdot r^2 h \gamma_{\mathcal{C},ls}(r)$  [see Eq. (63)]. The dotted blue and red curves are the plot of the error, multiplied by 15, in  $0 < r < 2R$  and  $r > 2R$ , respectively.

## 5 Scattering intensity behavior

The scattering intensity  $I(q)$  is the Fourier transform (FT) of equation (1) times  $V \langle \eta^2 \rangle$  and is, therefore, equal to

$$I(q) = \frac{4\pi V \langle \eta^2 \rangle}{q} \int_0^\infty r \sin(qr) \gamma(r) dr. \quad (65)$$

This can be recast into the form (Ciccariello & Riello, 2007)

$$I(q) = \frac{V}{2} \sum_{i=1}^3 n(i; j, k) \phi_i (1 - \phi_i) \tilde{\Gamma}_i(q) \quad (66)$$

with

$$\tilde{\Gamma}_i(q) \equiv \frac{4\pi}{q} \int_0^\infty r \sin(qr) \Gamma_i(r) dr. \quad (67)$$

The existence of the integral is ensured by condition (6b), while equation (6a) implies the following sum-rule

$$\int_0^\infty q^2 \tilde{\Gamma}_i(q) dq = 2\pi^2, \quad (68)$$

responsible for the Porod invariant relation

$$\mathcal{Q}_P \equiv \int_0^\infty q^2 I(q) dq = 2\pi^2 \langle \eta^2 \rangle. \quad (69)$$

Besides, the  $\tilde{\Gamma}_i(q)$ s obey the condition  $\tilde{\Gamma}_i(q) \geq 0$  whatever the scattering vector  $q$  because they are the FTs of the  $\Gamma_i(r)$ s that have a convolution structure owing to definitions (3) and (4). However, these conditions are not sufficient, on the basis of (65), to ensure the required positiveness of  $I(q)$  because some of the  $n(i; j, k)$ s can be negative. Hence, the last quantities have to obey appropriate constraints to ensure the positiveness of  $I(q)$ . This conclusion, that might look at first surprising, is a consequence of the functional density theorem that states that the correlation function is uniquely determined by the density value and the interaction potential. On the basis of this statement it is clear that the assignment of the sample internal geometry, equivalent to assigning the  $\tilde{\Gamma}_i(q)$ s, cannot be fully independent of the  $n_i$  values.

Each  $P_{i,i}(r)$  is determined by the length distribution of the chords that have both ends within the related phase. In most of the cases the distribution is not uniform but has a particular shape that naturally defines some length values  $L_1, \dots, L_M$  as the bounds of the ranges relevant to the small and the large distances asymptotic behaviors of  $P_{i,i}(r)$  as well as to the positions of possible peaks and shoulders. Since  $\Gamma_i(r)$  is obtained from  $P_{i,i}(r)$  by subtracting to this quantity  $\phi_i^2$  it happens that  $\Gamma_i(r)$  is certainly positive around the origin owing to (6a) and that it can be negative for other  $r$  values. The aforesaid distances  $L_1 < \dots < L_M$  in turns define some particular scattering vector values  $\bar{q}_i$  ( $i = 1, \dots$ ) through the well known relation  $\bar{q}_i = 2\pi/L_i$ . The  $\bar{q}_i$ s are the reciprocal space values where one expects a change in the  $\tilde{\Gamma}_i(q)$  behavior.

One applies now these considerations to the film-like and thread-like systems discussed in the previous sections. There it was shown that the  $P_{1,1}(r)$  SPF is certainly endowed of two typical lengths:  $\bar{R}_s$  [ $\bar{R}_c$ ] [see equations (15) and (48)] and  $\delta$  [ $2\delta$ ] with  $\bar{R}_s > \delta$  [ $\bar{R}_c > 2\delta$ ] and that  $P_{1,1}(r)$  is fairly approximated by a third degree polynomial if  $r < \delta$  [ $2\delta$ ] and by a surface [a curve] CF if  $r > \delta$  [ $2\delta$ ]. It is convenient to separately discuss the case of film-like systems and that of thread-like ones.

## 5.1 Intensity behavior in the film-like case

To begin with one analyzes first the behavior of  $\tilde{\Gamma}_1(q)$  under the further simplifying assumption that one only has two typical lengths, *i.e.*  $L_1 = \delta$  and  $L_2 = \bar{R}_s$ . Thus, the  $\tilde{\Gamma}_1(q)$  behavior is expected to change as one passes from

the  $q$ -range  $[0, 2\pi/\bar{R}_s]$  to  $[2\pi/\bar{R}_s, 2\pi/\delta]$  and, finally, to  $[2\pi/\delta, \infty]$ . By (3) and the results of §3 one finds that

$$\Gamma_1(r) \approx \begin{cases} \bar{\mathfrak{P}}_1(r) & \text{if } 0 < r < \delta \\ \bar{\gamma}_S(r) & \text{if } \delta < r, \end{cases} \quad (70)$$

where it has been put

$$\bar{\mathfrak{P}}_1(r) \equiv \frac{\mathfrak{P}_1(r) - \phi_1^2}{\phi_1(1 - \phi_1)}, \quad \text{and} \quad \bar{\gamma}_S(r) \equiv \frac{\delta^2 S_f \gamma_S(r)/V - \phi_1^2}{\phi_1(1 - \phi_1)}. \quad (71)$$

The FT of equation (70) yields

$$\tilde{\Gamma}_1(q) = \tilde{\mathfrak{P}}_1(q) + \tilde{\gamma}_S(q), \quad (72)$$

with

$$\tilde{\mathfrak{P}}_1(q) = \frac{4\pi}{q} \int_0^\delta r \sin(qr) \bar{\mathfrak{P}}_1(r) dr \quad (73)$$

and

$$\tilde{\gamma}_S(q) = \frac{4\pi}{q} \int_\delta^\infty r \sin(qr) \bar{\gamma}_S(r) dr. \quad (74)$$

[It is observed that condition (23) ensures that  $\bar{\gamma}_S(r) \rightarrow 0$  as  $r \rightarrow \infty$  so that integral (74) exists.] The behavior of  $\tilde{\Gamma}_1(q)$  within the first  $q$ -range  $[0, 2\pi/\bar{R}_s]$  could be obtained by expanding the function around  $q = 0$ . One finds

$$\tilde{\Gamma}_1(q) \approx \sum_{n=0}^N \frac{(-1)^n}{(2n+1)!} (M_{\mathfrak{P},2n} + M_{\gamma_S,2n}) q^{2n} + o(q^{2N}) \quad (75)$$

with

$$M_{\mathfrak{P},2n} \equiv \int_0^\delta r^{2n+3} \bar{\mathfrak{P}}_1(r) dr \quad (76)$$

and

$$M_{\gamma_S,2n} \equiv \int_\delta^\infty r^{2n+3} \bar{\gamma}_S(r) dr. \quad (77)$$

One sees that  $M_{2n} [\equiv (M_{\mathfrak{P},2n} + M_{\gamma_S,2n})]$  is the  $2n$ th moment of  $\Gamma_1(r)$ . Since  $M_{\mathfrak{P},2n}$  is  $O(\delta^{2n+3})$ , the value of  $M_{2n}$  is essentially equal to the corresponding momentum of  $\bar{\gamma}_S(r)$  and strongly depends on the way  $\bar{\gamma}_S(r)$  approaches zero as  $r \rightarrow \infty$ . Since the last behavior generally is not known, on a general ground the only existence and positiveness of  $M_0$  is certain. The existence of the other higher moments is certain only if one assumes that  $\bar{\gamma}_S(r)$  approaches zero by an exponential decrease or, more strongly, that the sample is a dilute

collection of particles with a finite maximal size and that the inter-particle interference may be neglected (Guinier & Fourn  t, 1955).

Consider now the second  $q$ -interval  $[2\pi/\bar{R}_s, 2\pi/\delta]$ . If  $q$  is close to  $2\pi/\bar{R}_s$ , contribution  $\tilde{\tilde{\mathfrak{P}}}_1(q)$  to  $\tilde{\Gamma}_1(q)$  can still, though less accurately, be approximated by the sum  $(M_{\mathfrak{P},0} - M_{\mathfrak{P},2}q^2/6 + \dots)$  [see (75)]. To estimate contribution  $\tilde{\tilde{\gamma}}_S(q)$  one must determine its asymptotic behavior as  $q \rightarrow \infty$ . Integrating equation (74) by parts one finds that the leading term is

$$\tilde{\tilde{\gamma}}_S(q) \approx \frac{4\pi}{q^2} \frac{\delta^3 S_f \gamma_S(\delta)/V - \delta \phi_1^2}{\phi_1(1 - \phi_1)} \cos(q\delta).$$

In this expression, the contribution related to  $(-\delta \phi_1^2)$  is canceled by the corresponding contribution present in  $\tilde{\tilde{\mathfrak{P}}}_1(q)$  since  $\tilde{\mathfrak{P}}_1(r)$  also presents the constant term  $-\phi_1^2$ . Thus one can write

$$\tilde{\tilde{\gamma}}_S(q) \approx \frac{4\pi}{q^2} \frac{\delta^3 S_f \gamma_S(\delta)/V}{\phi_1(1 - \phi_1)} \cos(q\delta). \quad (78)$$

provides one also writes

$$\tilde{\tilde{\mathfrak{P}}}_1(q) \approx (M'_{\mathfrak{P},0} - M'_{\mathfrak{P},2}q^2/6) + \dots \quad (79)$$

where the primes denote that the moments have been evaluated by (75) without subtracting  $\phi_1^2$  from  $\mathfrak{P}_1(r)$ . In the sub-interval of the considered  $q$ -range such that  $q\bar{R}_s > 2\pi$  and  $q\delta < 1$ , using (22) and the relation  $\delta S_f/V \approx \phi_1$ , from (78) one gets

$$\tilde{\tilde{\gamma}}_S(q) \approx \frac{2\pi}{q^2} \frac{\delta}{1 - \phi_1}. \quad (80)$$

Recalling that  $M'_{\mathfrak{P},0}$  is  $O(\delta^3)$  one finds that  $M'_{\mathfrak{P},0} \propto \delta(q\delta)^2/q^2$  that, compared to the above contribution, can be neglected. One concludes that

$$\tilde{\Gamma}_1(q) \approx \frac{2\pi}{q^2} \frac{\delta}{1 - \phi_1} \quad \text{if} \quad \frac{2\pi}{\bar{R}_s} < q < \frac{1}{\delta}. \quad (81)$$

Once one considers the third  $q$ -range, *i.e.*  $\frac{2\pi}{\delta} < q$ , in direct space the sample structure is analyzed on a distance scale smaller than  $\delta$ . Then, the limit  $\delta \rightarrow 0$  is no longer valid and the large  $q$  behavior of  $\tilde{\Gamma}_1(q)$  must be determined starting from the FT of  $\Gamma_1(r)$  defined by (3). An integration by parts and the use of (8) immediately yields the equivalent of the Porod relation

$$\tilde{\Gamma}_1(q) \approx \frac{4\pi S_f}{V \phi_1(1 - \phi_1) q^4} \quad \text{if} \quad \frac{2\pi}{\delta} < q. \quad (82)$$

Confining oneself to three phase film-like systems where film-like phase 1 fully separates phase 2 from phase 3 (so that the last two phases have no common interface), phases 2 and 3 are characterized by the only length  $\bar{R}_s$ . Then, by the same considerations that yielded (82), one concludes that the asymptotic leading terms of  $\tilde{\Gamma}_2(q)$  and  $\tilde{\Gamma}_3(q)$  are

$$\tilde{\Gamma}_i(q) \approx \begin{cases} O(\delta^3) & \text{if } q < \frac{2\pi}{\bar{R}_s} \quad i = 2, 3, \\ \frac{2\pi S_f}{V \phi_i(1-\phi_i) q^4}, & \text{if } \frac{2\pi}{\bar{R}_s} < q \quad i = 2, 3. \end{cases} \quad (83)$$

Substituting the above asymptotic behaviors within equation (65) it results that the asymptotic leading term of the scattering intensity relevant to a three-phase film-like system (with no common interface between phases 2 and 3) is

$$I(q) \approx \begin{cases} \frac{\mathcal{P}_S}{q^2} & \text{if } \frac{2\pi}{\bar{R}_s} < q < \frac{1}{\delta}, \\ \frac{\mathcal{P}}{q^4} & \text{if } \frac{2\pi}{\delta} < q. \end{cases} \quad (84)$$

with

$$\mathcal{P}_S \equiv \pi n(1; 2, 3) \delta^2 S_f, \quad (85)$$

$$\mathcal{P} \equiv 2\pi S_f ((n_1 - n_2)^2 + (n_1 - n_3)^2). \quad (86)$$

The main conclusion of this analysis is that: *if  $\delta \ll \bar{R}_s$ , the log-log plot of the scattering intensity of a three-phase film-like system shows a linear behavior with slope -2 at intermediate  $q$ -values and a further linear behavior with slope -4 in the outer  $q$ -range* (of course, provided  $q_{max}$ , the largest observed scattering vector, obeys to  $q_{max}\delta \gg 2\pi$ ). Hence, the lower bounds  $q_s$  and  $q_l$  of the two linear behavior ranges yield an estimate of  $\bar{R}_s$  and  $\delta$  through the relations  $\bar{R}_s \approx 2\pi/q_s$  and  $\delta \approx 2\pi/q_l$ . The intersections of the two straight lines with the vertical axis set at  $\log(q) = 0$  determine the values of  $\log(\mathcal{P}_S)$  and  $\log(\mathcal{P})$ . According to (85) and (86), the resulting ratio  $\mathcal{P}_S/\mathcal{P}$  determines  $\delta$  if the phase contrasts are known and then, either  $\mathcal{P}_S$  or  $\mathcal{P}$  can be used to determine the film area  $S_f$ .

The assumption that phases 2 and 3 have no common interface is now relaxed. Then, equations (81) and (82) remain unchanged while the second of equations (83) converts into

$$\tilde{\Gamma}_2(q) \approx \frac{2\pi(S_{1,2} + S_{2,3})}{V \phi_2(1 - \phi_2) q^4}, \quad \frac{2\pi}{\bar{R}_s} < q \quad (87)$$

and a similar one for  $\tilde{\Gamma}_3(q)$  with  $S_{1,2} + S_{1,3} = S_f$ . From these relations and (65) one obtains the general expressions of  $\mathcal{P}_S$  and  $\mathcal{P}$

$$\mathcal{P}_S \equiv \pi n(1; 2, 3) \delta^2 (S_{1,2} + S_{1,3}), \quad (88)$$

$$\mathcal{P} \equiv 2\pi [S_{1,2}(n_1 - n_2)^2 + S_{1,3}(n_1 - n_3)^2 + S_{2,3}(n_2 - n_3)^2]. \quad (89)$$

Though these two relations, even combined with the Porod invariant one, are no longer sufficient to determine the four structural parameters  $\delta$ ,  $S_{1,2}$ ,  $S_{1,3}$  and  $S_{2,3}$ , they yield however useful general bounds on these parameters. Two illustrations are now reported. Although they are naïve mathematical models they illustrate the main points of the previous discussion. The first illustration deals with the scattering intensity of a spherical shell whose  $(R, \delta)$  parameters take the values:  $(1, 0.02)u$  and  $(0.5, 0.1)u$ . The left panel

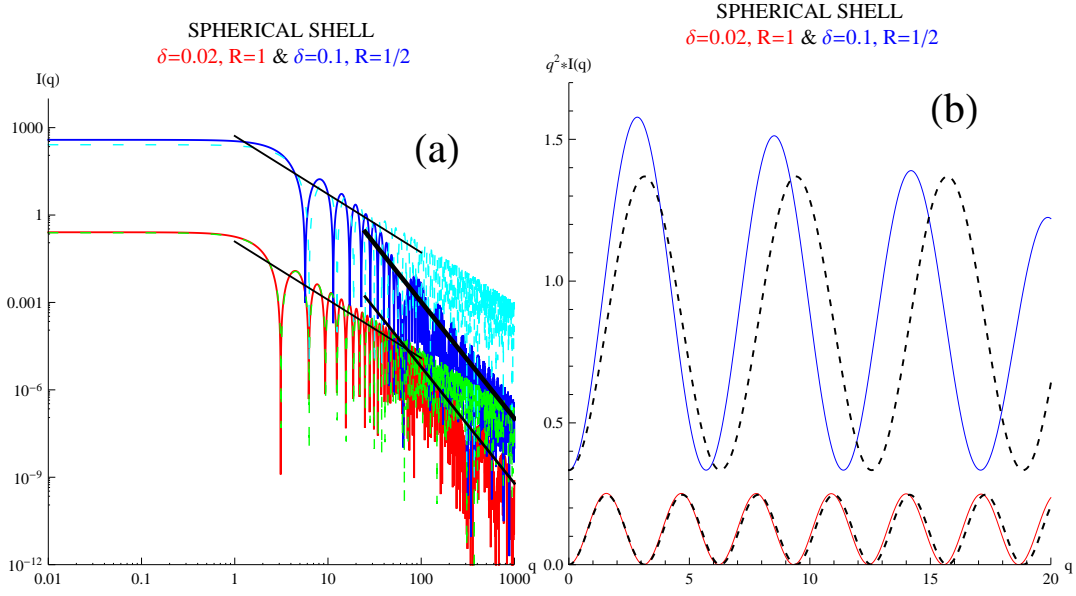


Figure 4: (a) The red and the blue curve are the plots of the FTs of equation (40) with  $(R, \delta)$  respectively equal to  $(1, 0.02)u$  and  $(0.5, 0.1)u$ , while the green and the cyan curves are the FTs of (41). The blue and the cyan intensities have been multiplied by  $10^3$  for greater clarity. (b) Kratky plots of the previous intensities. The dotted curves refer to the FTs of (41). The blue curves have vertically been shifted by 0.3. The agreement improves as  $\delta/R$  gets smaller. [The  $q$  units are  $u^{-1}$ .]

of Fig. 4 shows, in red and blue, the spherical shells' scattering intensities obtained by the FT of (40) and, in cyan and green, the corresponding FTs of  $\frac{\delta^2 S_1}{V} \gamma_{S, sph}(r, R)$  [see (41)], equal to

$$\frac{\delta^2 S_1}{V} \tilde{\gamma}_{S, sph}(q) = 12\pi R^2 \delta \sin^2(qR) / [q^2(3R^2 + 3R\delta + \delta^2)]. \quad (90)$$

[This FT has been obtained by integrating over  $[0, 2R]$ , the total support of  $\gamma_{S, sph}(r, R)$ .] The thin and the thick continuous straight lines are the plots of the leading asymptotic terms given by equation (84) [and (85) and (86)].



The figure shows that the intensity relevant to the spherical shell [leaving aside the oscillations] shows both a  $q^{-2}$  and a  $q^{-4}$  behavior and that the intensity of the associated spherical surface well reproduces the first intensity throughout the range  $[0, 2\pi/\delta]$  (*i.e.* not only within  $[2\pi/\bar{R}_s, 2\pi/\delta]$ ). Moreover it results that the smaller the ratio  $\delta/2R$  the wider becomes the range where the  $q^{-2}$  behavior occurs. The right panel of Fig. 4 shows the  $q^2 I(q)$  versus  $q$  plots (also known as Kratky plots) of the two considered spherical shells (continuous curves) and of their associated spherical surfaces (broken curves). The agreement is much better in the case  $(1, 0.02)$  owing to the smaller  $\delta/2R$  value.

The second illustration deals with the case of two disk-like cylinders char-

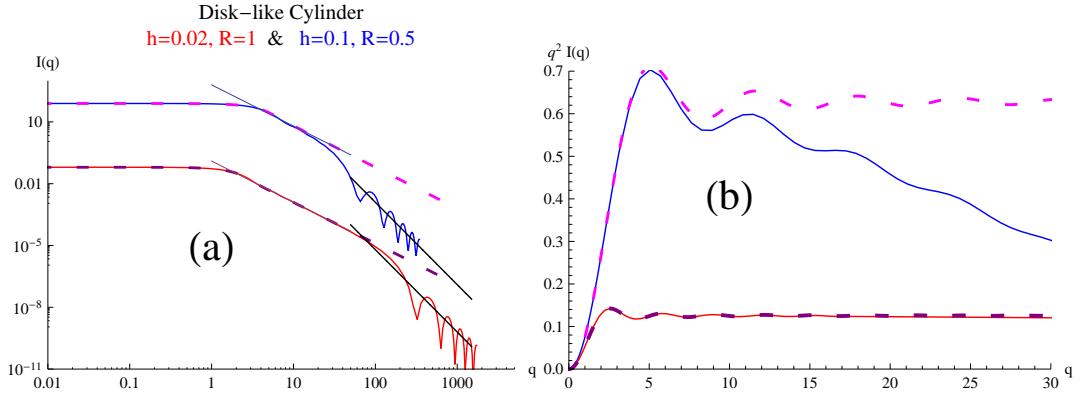


Figure 5: (a): The red and the blue curve are the plots of the FTs of equation (108) with  $(R, h)$  respectively equal to  $(1, 0.02)u$  and  $(0.5, 0.1)u$ , while the magenta and the purple curves are the associated FTs of (41). The blue and the magenta intensities have been multiplied by  $10^3$  for greater clarity; (b): Kratky plots of the previous intensities (without any scaling factor). The broken curves refer to equation (91).

acterized by  $(h, R) = (0.02, 1)u$  and  $(h, R) = (0.1, 0.5)u$ . The corresponding intensities are obtained by numerically Fourier transforming equation (108) and respectively yield the red and the blue continuous curves shown in Fig. 5a. The associated surface-like intensities are the 3D FTs of (42) multiplied by  $h^2 S_f/V$ , *i.e.*

$$\frac{h^2 S_f}{V} \tilde{\gamma}_{S,crcl}(q) = \frac{2h\pi}{q^2} \left[ 1 - J_0(2qR) - J_2(2qR) \right]. \quad (91)$$

Their plots are shown as magenta and purple broken curves. They practically superpose to the red and blue curves throughout  $[0, 2\pi/\delta]$ . The black lines are the plots of the relevant leading asymptotic behaviors given by (84).

One again observes that the  $q$ -range, where the intensity behavior is  $1/q^2$  becomes wider as  $h/R$  decreases. In the outer  $q$  range, as expected, the surface approximation no longer works since the intensity behaves as  $1/q^4$  in agreement with Porod's law. Fig. 5b allows one to better appreciate how the agreement between the particle and the surface-like intensities improves throughout  $0 < q < 2\pi/h$  as  $h/R$  decreases.

## 5.2 Intensity behavior in the thread-like case

Though, in most cases, a thread-like phase exists in presence of another single phase, hereafter one assumes that it exists in presence of two further phase and that the thread-like phase portion that lies on the interface between phases 2 and 3 is negligible so as to have  $L = L_2 + L_3$ , where  $L_2$  and  $L_3$  respectively denote the total lengths of the threads that fully lie within phases 2 and 3. It is also assumed that

$$S_{2,3} \gg S_{1,2} \quad \text{and} \quad S_{2,3} \gg S_{1,3} \quad (92)$$

and that the mean of the curvature radii of  $S_{2,3}$  is not smaller than  $\bar{R}_c$ , defined by (48). The above assumptions amount to say that the threads are in an extended configuration and that the mean distance among them is not smaller than  $\bar{R}_c$ . These properties make it possible to apply the considerations made in § 5.1 to the thread-like case. Thus, the equation equivalent of (74) and (71b) becomes

$$\tilde{\gamma}_c(q) = \frac{4\pi}{q} \frac{\sigma^2 L}{\phi_1(1-\phi_1)V} \int_{2\delta}^{\infty} r \sin(qr) \gamma_c(r) dr. \quad (93)$$

By (60), considering the only leading term, one finds

$$\tilde{\gamma}_c(q) \approx \frac{2\sigma^2 L}{V\phi_1(1-\phi_1)q} \int_{2q\delta}^{\infty} \frac{\sin(x)}{x} dx \approx \frac{2\sigma^2 L}{V\phi_1(1-\phi_1)q} \left[ \frac{\pi}{2} - \text{Si}(2q\delta) \right], \quad (94)$$

where  $\text{Si}(x)$  is the sine integral function (Gradshteyn & Ryzhik, 1980) that, at small  $x$ , behaves as  $-x$ . One concludes that

$$\tilde{\gamma}_c(q) \approx \tilde{\Gamma}_1(q) \approx \frac{\pi\sigma^2 L}{V\phi_1(1-\phi_1)q} \quad \text{if} \quad \frac{2\pi}{\bar{R}_c} < q < \frac{\pi}{\delta}. \quad (95)$$

In this  $q$ -range the  $\tilde{\Gamma}_i(q)$ s with  $i = 2, 3$  are negligible since they are  $O(\delta^3)$ . In the range  $q > 2\pi/\delta$  the behaviors are similar to those found in the film-like case. One finds

$$\tilde{\Gamma}_1(q) \approx \frac{2\pi(S_{1,2} + S_{1,3})}{V\phi_1(1-\phi_1)q^4}, \quad \text{if} \quad \frac{\pi}{\delta} < q, \quad (96)$$

and

$$\tilde{\Gamma}_i(q) \approx \frac{2\pi(S_{1,i} + S_{1,j})}{V\phi_i(1 - \phi_i)q^4}, \quad i \neq j = 2, 3 \quad \text{if} \quad \frac{2\pi}{\bar{R}_c} < q. \quad (97)$$

By (95), (96), (97) and (65) the asymptotic behavior of the thread-like scattering intensity is

$$I(q) \approx \begin{cases} \frac{\mathcal{P}_c}{q} & \text{if} \quad \frac{2\pi}{\bar{R}_c} < q < \frac{\pi}{\delta}, \\ \frac{\mathcal{P}}{q^4} & \text{if} \quad \frac{\pi}{\delta} < q. \end{cases} \quad (98)$$

with

$$\mathcal{P}_c \equiv \frac{\pi n(1; 2, 3)\sigma^2 L}{2} = \frac{\pi n(1; 2, 3)\sigma \phi_1 V}{2} \quad (99)$$

and  $\mathcal{P}$  given by (89).

The main consequence of this analysis is that the *log-log* plot of the scattering

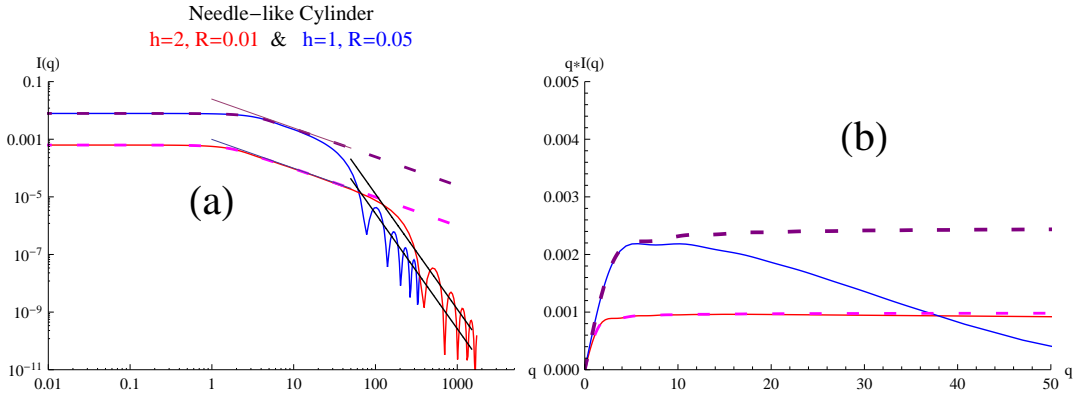


Figure 6: The two panels, similarly to Fig. 5, show the log-log plot and the  $qI(q)$  versus  $q$  plots of the intensities relevant to two needle-like cylinders of height ( $h$ ) and radius ( $R$ ) as specified at the top of panel (a) as well as their thread-like approximation given by (100).

intensity of a thread-like sample may show a linear behavior with slope -1 at intermediate  $q$  values and another linear behavior with slope -4 (*i.e.* the Porod one) at larger  $q$ s. The associated constants  $\mathcal{P}_c$  and  $\mathcal{P}$  are related to the the section and the length of the thread-like phase, the scattering contrasts and the interface surface areas as reported in (99) and (88). The expressions immediately convert to the two phase case ones by setting  $n_3 = n_2$  and  $S_{2,3} = 0$ . In this way the  $\mathcal{P}_c$  expression reduces to that obtained by Kirste & Oberthür (1988) under the more restrictive assumption that the particles are rod-like. In particular, in the two phase case, the determination of  $\mathcal{P}_c$  and  $\mathcal{P}$  allows one to determine the normal section and the total surface areas

of the thread-like phase if one knows the contrast because volume fraction  $\phi_1$  can be obtained by the Porod invariant value [*i.e.* equation (69)].

Figure 6 reports an illustration of these results considering the case of a needle-like cylinder, *i.e.* a cylinder with its height  $h$  larger than its diameter  $2R$ . The scattering intensity is obtained by the numerical integration of (109). The intensity associated to the limit  $\sigma \rightarrow 0$  of the thread like phase is obtained, according to (52), multiplying by  $h\sigma^2/V$  the FT of (63). In this way one finds

$$\frac{h\sigma^2}{V} \tilde{\gamma}_{C,ls}(q) = \frac{2\sigma}{h q^2} \left[ \cos(hq) + (hq) \text{Si}(hq) - 1 \right], \quad (100)$$

where  $\text{Si}(x)$  is the sine integral function. The expression on the right hand side approaches  $\pi h R^2$  as  $q \rightarrow 0$  and behaves as  $\pi^2 R^2/q$  in the range  $qh \gg 1$ . The figure shows that the region where the intensity behaves as  $1/q$  enlarges as the  $R/h$  ratio decreases. Actually, as in the previously reported cases, this value must be smaller than few percents for the  $q^{-1}$  behavior to be clearly observed.

### 5.3 The right parallelepiped case

It may happen that a given sample appears as made up of threads if observed on a coarse length scale and of films if observed on a fine one. Then, its scattering intensity will show both a  $q^{-1}$  and a  $q^{-2}$  behavior, besides the  $q^{-4}$  one at very large  $qs$ . A dilute monodisperse and statistically isotropic sample made up of right parallelepipeds of sizes  $a \times b \times c$  with  $a \ll b \ll c$ , is a paramount example of this phenomenon, as it will now be shown. The monodispersity assumption allows one to confine the attention to the behaviors of the CF and the form factor of a single parallelepiped. The CF of this particle shape was worked out by Gille (1999) and has an analytic form. Since one expects that the parallelepiped looks as a linear segment on a length scale greater than  $b$  (and smaller than  $c$ ) and as a rectangle on a scale greater than  $a$  (and smaller than  $b$ ), from equations (52) and (20) it follows that

$$\gamma_{V,prl}(r) \approx \begin{cases} \frac{(ab)^2 c}{abc} \gamma_{C,ls}(r, c) & \text{if } b < r < c \\ \frac{a^2 bc}{abc} \gamma_{S,rect}(r; b, c) & \text{if } a < r < b, \end{cases} \quad (101)$$

where  $\gamma_{V,prl}(r)$  is the parallelepiped CF reported by Gille (1999),  $\gamma_{C,ls}(r, c)$  the linear segment CF given by (63) and  $\gamma_{S,rect}(r; b, c)$  the rectangle surface CF given by equation (44). Figure 8a shows the accuracy achieved by (101) in approximating the CF of a right parallelepiped with  $a = 1/100u$ ,  $b = 1u$

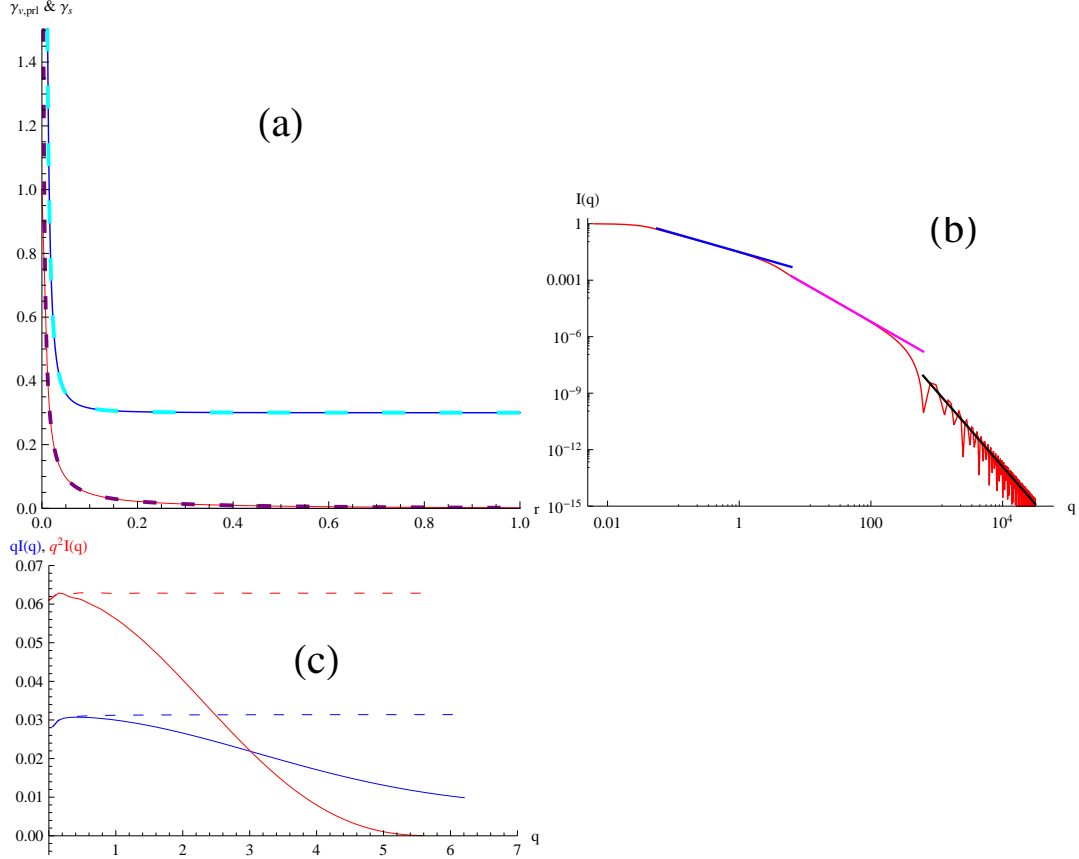


Figure 7: (a) Behavior of the parallelepiped CF and its thread and film-like approximations; (b) behavior of the scattering intensity and its leading  $q^{-1}$ ,  $q^{-2}$  and  $q^{-4}$  "asymptotic" terms; (c) behavior of the  $qI(q)$  (blue) and  $q^2I(q)$  (red) versus  $q$  plots of the parallelepiped intensity (continuous curves) and of the relevant curve and surface intensity approximations (broken curves).

and  $c = 100u$  by the relevant film and thread CFs. In fact, the continuous red curve is the plot of  $\gamma_{V,prl}(r)$  and the broken magenta one that of  $a \cdot \gamma_{S,rect}(r; b, c)$  throughout the range  $a < r < b$ . The continuous blue curve is the plot of  $10^3 \cdot \gamma_{V,prl}(r)$  and the broken cyan one that of  $10^3 \cdot ab \cdot \gamma_{C,ls}(r, c)$  throughout  $b < r < c$  (this interval has been linearly mapped over  $[0.01, 1]$ , and both curves are vertically shifted by 0.3). The form factor  $I_{V,prl}(q)$  of the considered parallelepiped is the red curve shown in fig. 8b and is numerically obtained evaluating the FT of  $\gamma_{V,prl}(r)$ . The blue, the magenta and the black linear segments, which respectively behave as  $q^{-1}$ ,  $q^{-2}$  and  $q^{-4}$ , have been obtained by equations (98a), (84a) and (98b) [or (84b)]. They have been drawn within the  $q$ -ranges:  $[2\pi/c, 2\pi/b]$ ,  $[2\pi/b, 2\pi/a]$  and  $[2\pi/a, 6 \cdot 10^4 u^{-1}]$ . One sees that

the  $q^{-1}$  and  $q^{-2}$  behaviors are fairly obeyed close to the lower bounds of the previous two  $q$  intervals. In the proximity of the two upper bounds, the intensity deviates from the reported two linear behaviors as it appears more evident in figure 8c. Here the continuous and broken blue are the plots of  $q I_{V,prl}(q)$  and of  $abq\tilde{\gamma}_{C,ls}(q, c)$  [note that, similarly to the previously reported cases, this FT has been evaluated integrating over the full support of  $\gamma_{C,ls}(r, c)$  to ensure its positiveness] within the  $[2\pi/c, 2\pi/b]$   $q$ -range, and the continuous and broken red curves are the Kratky plots of  $I_{V,prl}(q)$  and the FT of  $ab\tilde{\gamma}_{S,rect}(q; b, c)$  (evaluated over  $[0, \sqrt{b^2 + c^2}]$ ) within  $[2\pi/b < q < 2\pi/a]$  (the last interval has been linearly mapped over the former one).

## 6 Conclusion

The reported analysis has shown that the CF of a thread-like or a film-like statistically isotropic sample can be approximated by a 3rd degree polynomial in an inner distance range and, externally to this, by the associated curve or surface CF. The curve and the surface CFs respectively behave as  $1/r^2$  and as  $1/r$  close to the origin. Consequently, the relevant scattering intensities respectively behave as  $\mathcal{P}_C/q$  or as  $\mathcal{P}_S/q^2$  in a range of intermediate  $qs$  and as  $\mathcal{P}/q^4$  in the outer  $q$  range. The  $\mathcal{P}$  and  $\mathcal{P}_S$  expressions were determined by Porod (1951) and by Teubner (1990). The expression of  $\mathcal{P}_C$  is new. Both  $\mathcal{P}_S$  and  $\mathcal{P}_C$  coincide with the expressions obtained by Porod (1982) and by Kirste & Oberthür (1982) in the cases of plane lamellae and circular rods. On a practical ground, coefficients  $\mathcal{P}$  and  $\mathcal{P}_C$  or  $\mathcal{P}_S$  can easily be determined from the linear portions of the intensity log-log plot. Their knowledge determines, in a (nearly) model independent way, the interface area as well as the normal thread section area or the film thickness. Furthermore, a numerical check on the physical consistency of the assumed film-like or thread-like structure is possible because the lower bound of the  $q$ -range where the  $q^{-2}$  or  $q^{-1}$  behavior occurs must be close to the film thickness value or to the thread maximal chord value (estimated from the normal section area), respectively determined by  $\mathcal{P}_S$  and  $\mathcal{P}_C$ . The model illustrations, reported in § 3.4.1, 3.4.2 and 4.1.1, suggest that the linear behaviors in the log-log plots are observable if the two typical lengths,  $\delta$  and  $\bar{R}_s$  for the film-like case and  $2\delta$  and  $\bar{R}_c$  for the thread-like one, differ at least by an order of magnitude. This fact is confirmed by Figures 5 and 6. The paper analysis also applies to three phase systems. In this case of film-like samples involving three phases, the knowledge of coefficients  $\mathcal{P}_S$ ,  $\mathcal{P}$  and  $\mathcal{Q}_P$  only puts some bounds on the involved structural parameters since it is not sufficient to uniquely determine them. Whenever the scattering intensity is collected over a wider  $q$ -range,

as it happens using also ultra-small scattering equipments, one might study samples that behave in a thread-like way in the innermost  $q$ -range and in a film-like one in the intermediate  $q$ -range (see the model illustration reported in § 5.3). In this case, a trivial extension of the above analysis makes it possible to determine both the thread section area and the film thickness of the analyzed sample.

## Appendix A: the circular cylinder CF

The chord length distribution (CLD) of a circular right cylinder of radius  $R$  and height  $h$  is since long known (Gille, 2014). It involves the elliptic integral functions  $E(\varphi, k)$  and  $F(\varphi, k)$  as well as the complete elliptic integrals  $\mathbf{E}(k)$  and  $\mathbf{K}(k)$  [we are adopting here Gradsteyn & Ryzhik's (1980) definitions]. Besides, it is known that the CLD takes two different form depending on whether the cylinder has a disk-like form (*i.e.*  $h < 2R$ ) or a needle-like one (*i.e.*  $2R < h$ ). In the following two subsection one reports the explicit expressions of the CF that so far were never written down.

To this aim, one first puts

$$\Delta_1 \equiv \sqrt{4R^2 - r^2}, \quad \Delta_2 \equiv \sqrt{r^2 - h^2}, \quad \Delta_3 \equiv \sqrt{4R^2 + h^2 - r^2} \quad (102)$$

$$\mathcal{G} \equiv \frac{1}{24\pi r h R^2}, \quad \xi \equiv \frac{r}{2R}, \quad \zeta \equiv \frac{2hR}{r\Delta_3}, \quad (103)$$

$$\varphi_1 = \arcsin \xi, \quad \varphi_2 \equiv \arcsin \zeta, \quad (104)$$

$$\varphi_3 \equiv \arcsin \frac{\Delta_2}{2R}, \quad \varphi_4 \equiv \arcsin \frac{r\Delta_3}{2hR}, \quad (105)$$

$$G_A(r, R, h) \equiv \mathcal{G} \left[ 3 \left( r(4\pi R^2(2h - r) + (r^2 + 2R^2)\Delta_1) + \right. \right. \quad (106) \\ \left. \left. 8R^2(r^2 - R^2)\varphi_1 \right) - 16hR((r^2 + 4R^2)\mathbf{E}(\xi) + (r^2 - 4R^2)\mathbf{K}(\xi)) \right]$$

and

$$G_C(r, R, h) \equiv \mathcal{G} \left[ 12\pi R^2(h^2 + r^2 - R^2) - \right. \quad (107) \\ \left. (h^2 - 5r^2 - 26R^2)\Delta_2\Delta_3 - 24R^2(h^2 + r^2 - R^2)\varphi_3 - \right. \\ \left. 8hr \left( (r^2 + 4R^2)\mathbf{E}(\varphi_4, \frac{1}{\xi}) - (r^2 - 4R^2)\mathbf{F}(\varphi_4, \frac{1}{\xi}) \right) \right].$$

## The disk case

Then, integrating twice the CLD expression (see the deposited part), in the disk case [*i.e.*  $h < 2R$ ] one finds that the cylinder CF reads

$$\gamma_{disk}(r, R, h) = \begin{cases} G_A(r, R, h) & \text{if } 0 < r < h, \\ \mathcal{G} \left[ 12\pi h^2 R^2 + 3r(r^2 + 2R^2)\Delta_1 + \right. \\ \quad \left. \frac{\Delta_2}{\Delta_3}(3r^4 - h^4 + 6r^2(h^2 - R^2) + 22h^2 R^2 - 24R^4) + \right. \\ \quad \left. 24R^2((r^2 - R^2)\varphi_1 - (h^2 + r^2 - R^2)\varphi_3) - \right. \\ \quad \left. 16hR((r^2 + 4R^2)\mathbf{E}(\varphi_2, \xi) + (r^2 - 4R^2)\mathbf{F}(\varphi_2, \xi)) \right] & \text{if } h < r < 2R, \\ G_C(r, R, h) & \text{if } 2R < r < \sqrt{4R^2 + h^2}, \\ 0 & \text{if } \sqrt{4R^2 + h^2} < r. \end{cases} \quad (108)$$

## The needle case

Similarly, in the needle case [*i.e.*  $2R < h$ ], the CF is found to be

$$\gamma_{ndl}(r, R, h) = \begin{cases} G_A(r, R, h) & \text{if } 0 < r < 2R, \\ 4\mathcal{G} \left[ 3\pi R^2(2hr - R^2) - \right. \\ \quad \left. 2hr \left( (r^2 + 4R^2)\mathbf{E}(\frac{1}{\xi}) - (r^2 - 4R^2)\mathbf{K}(\frac{1}{\xi}) \right) \right] & \text{if } 2R < r < h, \\ G_C(r, R, h) & \text{if } h < r < \sqrt{4R^2 + h^2}, \\ 0 & \text{if } \sqrt{4R^2 + h^2} < r. \end{cases} \quad (109)$$

## Appendix B: the cubic surface CF

In deriving equation (32) it was implicitly assumed that the given surface intersects its translated image along a curve. In the reality it can happen that for some translation directions the intersection be a surface subset. An illustration of this phenomenon is shown in Figure 8 that refers to a cubic surface of area  $S_f = 6a^2$ . The red polygon, shown in Fig. 8a, is the intersection set of the outset cubic surface with its image resulting by the translation of the cubic surface by  $r\hat{\omega}$ . This vector is such that its tip point does not lie over one of the cube faces. The case where  $r\hat{\omega}$  fully lies over one of the cube faces leads to an intersection set that is formed by two surfaces that respectively have their borders equal to the red thick continuous and broken rectangles shown in Fig.8b. When the only tip of  $r\hat{\omega}$  spans one of the cube



faces the intersection set is again a surface whose boundary is given by the red rectangle shown in Fig. 8c. To get the CF of the cubic surface it is necessary to evaluate integral (21) imposing the aforesaid constraints on  $r\hat{\omega}$ . This task was explicitly carried out as detailed in the deposited part of this paper. Here one simply reports the surface CF expressions relevant to the geometrical configurations illustrated in first three panels of Fig. 8.

They respectively read

$$\gamma_{S,CS,a}(r,a) \equiv \begin{cases} \frac{1}{a} - \frac{r}{2a^2} & \text{if } 0 < r < a, \\ \frac{5}{2r} - \frac{2}{a} - \frac{2\sqrt{r^2-a^2}}{\pi ar} + \frac{2r}{\pi a^2} \arccos \frac{a}{r} & \text{if } a < r < \sqrt{2}a, \\ \frac{5\pi-12}{6\pi r} - \frac{2}{a} + \frac{r}{6a^2} + \frac{2\sqrt{r^2-2a^2}}{\pi ar} + \frac{4}{\pi a} \arcsin \left( \frac{r^2+a^2}{r^2-a^2} \sqrt{\frac{r^2-2a^2}{2r^2-2a^2}} \right) + \frac{2(r^2+5a^2)}{3\pi a^2 r} \arcsin \left( \frac{7a^3-3ar^2}{(r^2-a^2)^{3/2}} \right) & \text{if } \sqrt{2}a < r < \sqrt{3}a, \\ 0 & \text{if } \sqrt{3}a < r, \end{cases} \quad (110)$$

$$\gamma_{S,CS,b}(r,a) \equiv \begin{cases} \frac{1}{2r} - \frac{2}{\pi a} + \frac{r}{2\pi a^2} & \text{if } 0 < r < a, \\ -\frac{2+\pi}{2\pi r} - \frac{r}{2\pi a^2} + \frac{2\sqrt{r^2-a^2}}{\pi ar} + \frac{2}{\pi r} \arcsin \left( \frac{a}{r} \right) & \text{if } a < r < \sqrt{2}a, \\ 0 & \text{if } \sqrt{2}a < r. \end{cases} \quad (111)$$

and

$$\gamma_{S,CS,c}(r,a) \equiv \begin{cases} 0 & \text{if } 0 < r < a, \\ \frac{\pi-1}{2\pi r} + \frac{r}{2\pi a^2} - \frac{2\sqrt{r^2-a^2}}{\pi ar} & \text{if } a < r < \sqrt{2}a, \\ -\frac{1}{2\pi r} - \frac{r}{2\pi a^2} + \frac{2}{\pi ar} \sqrt{r^2-2a^2} - \frac{1}{\pi r} \arcsin \left( \sqrt{\frac{r^2-2a^2}{r^2-a^2}} \right) + \frac{1}{\pi r} \arcsin \left( \sqrt{\frac{a}{r^2-a^2}} \right) & \text{if } \sqrt{2}a < r < a\sqrt{3}, \\ 0 & \text{if } \sqrt{3}a < r. \end{cases} \quad (112)$$

Thus, the CF function of a cubic surface is the sum of equations (110), (111) and (112). Its first moment is equal to  $6a^2/4\pi$ , as required by equation (30) while its plot is shown in panel (d) of Fig. 8 for the case  $a = 1$ . The discontinuity, present at  $r = a$ , arises from the opposite faces that are parallel at distance  $a$ .

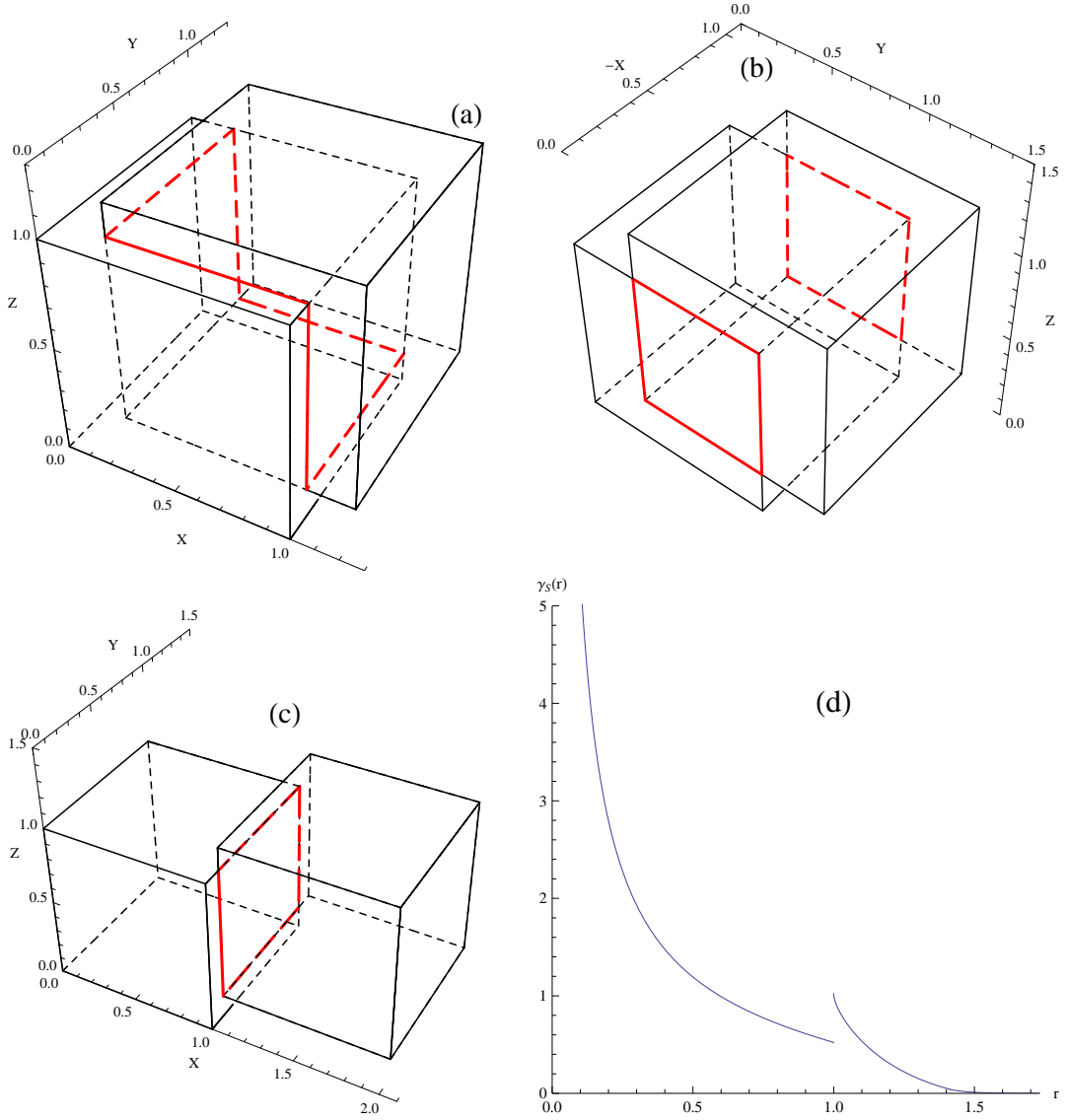


Figure 8: If  $r\hat{w}$  is such that the tip of  $r\hat{w}$  does not lie on one of the cube's faces, the intersection of the outset and the translated cubic surfaces is made up of the continuous and broken thick segments shown in panel (a). If  $r\hat{w}$  is such that  $\theta$  is equal to 0 or  $\frac{\pi}{2}$  or  $\pi$ , so as to have two pairs of faces sliding one over the other, the intersection set is formed by two opposite rectangles having as borders the continuous and the broken thick red curves shown in the (b) panel that explicitly refers to the case  $\theta = 0$ . Finally, if  $r\hat{w}$  is such that its tip point spans one of the cube's face, the intersection set is formed by the rectangle shared by the superposing faces, *i.e.* the rectangle having as border the rectangular curve show in red in panel (c). Panel (d) shows the final cubic surface CF given by the sum of the aforesaid three contributions.

## Appendix C: small distance behavior of the curve CF

In order to prove equation (60) one proceeds by expanding the parametric equation of the curve around  $\ell = 0$  which is the curvilinear coordinate of the point taken as the origin of the Cartesian frame. The expansion up to terms  $o(\ell^3)$  reads

$$\mathbf{R}(\ell) \approx \left\{ \ell - \frac{\ell^3}{6 R_c^2}, \frac{\ell^3}{6 R_c R_t}, \frac{\ell^2}{2 R_c} \right\}. \quad (113)$$

One straightforwardly verifies that vectors  $\hat{\tau}$ ,  $\hat{\mathbf{n}}$  and  $\hat{\mathbf{b}}$ , obtained by applying definitions (46) to (113) are mutually orthogonal unit vectors up to terms  $o(\ell^3)$ . The condition  $\mathbf{R}(\ell) \cdot \mathbf{R}(\ell) = r^2$  determines the curvilinear abscissa of the points that are at distance  $r$  from the origin. As  $r \rightarrow 0$ , the equation is easily solved by iteration, putting  $l \approx r$  as first step. The solutions are

$$\ell_{\pm} \approx \pm r \left( 1 + \frac{r^2}{24 R_c^2} \right) + O(r^5). \quad (114)$$

Consider the positive solution. One finds that  $\hat{\omega}(\ell_+) = \mathbf{R}(\ell_+)/r$  and  $\hat{\tau}(\ell_+) = \frac{d\mathbf{R}(\ell)}{d\ell} \Big|_{\ell=\ell_+}$ . In this way, by equation (57), one obtains

$$\cos \theta_+ = \hat{\omega}(\ell_+) \cdot \hat{\tau}(\ell_+) \approx 1 - \frac{r^2}{8 R_c^2} + o(r^2). \quad (115)$$

The result for the negative solution is the same. In this way result (60) is immediately obtained by (59).

## Acknowledgments

We gratefully thank Dr. Wilfried Gille for his critical reading of the ms and for the suggestion of investigating the moments of the curve and the surface CFs.

## References

- Avdeev, M. V., Aksenov, V. L., Gazová, Z., Almsy, L., Petrenko, V. I., Gojzewski, H., Feoktystov, A. V., Siposova, K., Antosova, A., Timko M. & Kopcansky, P. (2013). *J. Appl. Cryst.* **46**, 224-233.
- Ciccariello, S. (1984). *J. Appl. Phys.* **56**, 162-167.
- Ciccariello, S. (1989). *Acta Cryst. A* **45**, 86-99.
- Ciccariello, S. (1991). *Phys. Rev. A* **44**, 2975-2983.
- Ciccariello, S. (1995). *J. Math. Phys.* **36**, 219-246.
- Ciccariello, S. (2009). *J. Math. Phys.* **50**, 103527/20.
- Ciccariello, S. (2010). *J. Appl. Cryst.* **43**, 1377-1384.
- Ciccariello, S. (2014). *J. Appl. Cryst.* **47**, 1866-1881.
- Ciccariello, S. & Benedetti, A. (1982). *Phys. Rev.* **B26**, 6384-6389.
- Ciccariello, S. & Riello, P. (2007). *J. Appl. Cryst.* **40**, 282-289.
- Ciccariello, S. & Sobry, R. (1995). *Acta Cryst. A* **51**, 60-69.
- Ciccariello, S., Cocco, G., Benedetti, A. & Enzo, S. (1981). *Phys. Rev.* **B23**, 6474-6485.
- Debye, P., Anderson, H.R. & Brumberger, H. (1957). *J. Appl. Phys.* **20**, 679-683.
- Fedorova, I.S. & Emelyanov, V.B. (1977). *J. Colloid Interface Sci.* **59**, 106-112.
- Feigin, L.A. & Svergun, D.I. (1987). *Structure Analysis by Small-Angle X-Ray and Neutron Scattering*, New York: Plenum Press.
- Gille, W. (1999). *J. Appl. Cryst.* **32**, 1100-1104.
- Gille, W. (2014). *Particle and Particle Systems characterization*, London: CRC.
- Goodisman, J. & Brumberger, H. (1971). *J. Appl. Cryst.* **4**, 347-351.
- Glatter, O. (1982). *Small-Angle X-Ray Scattering*. Edts Glatter, O. & Kratky, O., London: Academic Press.

- Gradshteyn, I.S. & Ryzhik, I.M. (1980). *Tables of Integrals, Series and Products*, New York: Academic Press.
- Guinier, A. & Fournet, G. (1955). *Small-Angle Scattering of X-rays*. New York: John Wiley.
- Kirste, R.G. & Porod, G. (1962). *Kolloid Z.* **184**, 1-6.
- Kirste, R.G. & Oberthür, R.C. (1982). *Small-Angle X-Ray Scattering*. Eds Glatter, O. & Kratky, O., London: Academic Press
- Kostorz, G. (1979). *Neutron Scattering*, Ed. Kostorz, G., London: Academic Press, pp 227-289.
- Melnichenko, Y.B. & Ciccariello, S. (2012). *J. Phys. Chem. C* **116**, 24661-24671.
- Méring, J. & Tchoubar, D. (1968). *J. Appl. Cryst.* **1**, 153-65.
- Peterlin, A. (1965). *Makromol. Chem.* **87**, 152-160.
- Porod, G. (1951). *Kolloid Z.* **124**, 83-114.
- Porod, G. (1967). *Small-Angle X-Ray Scattering. Proceedings of the Syracuse Conference*, Ed. H. Brumberger, 1-8, New York: Gordon & Breach.
- Porod, G. (1982). *Small-Angle X-Ray Scattering*. Eds Glatter, O. & Kratky, O., London: Academic Press.
- Smirnov, V.I. (1970). *Cours de Mathématiques Supérieures*, Moscow: Mir, Vol. II, Chap. V.1.
- Teubner, M. (1990). *J. Chem. Phys.* **92**, 4501-4507.
- Wu, H. & Schmidt, P. W. (1974). *J. Appl. Cryst.* **7**, 131-146.